

Early Holocene temperature variability in the Nordic Seas: The role of oceanic heat advection versus changes in orbital forcing

Bjørge Risebrobakken,^{1,2} Trond Dokken,^{1,2} Lars Henrik Smedsrud,^{1,2} Carin Andersson,^{1,2,3}
Eystein Jansen,^{1,2,3} Matthias Moros,^{2,4} and Elena V. Ivanova⁵

Received 7 January 2011; revised 15 July 2011; accepted 21 July 2011; published 22 October 2011.

[1] The separate roles of oceanic heat advection and orbital forcing on influencing early Holocene temperature variability in the eastern Nordic Seas is investigated. The effect of changing orbital forcing on the ocean temperatures is tested using the 1DICE model, and the 1DICE results are compared with new and previously published temperature reconstructions from a transect of five cores located underneath the pathway of Atlantic water, from the Faroe-Shetland Channel in the south to the Barents Sea in the north. The stronger early Holocene summer insolation at high northern latitudes increased the summer mixed layer temperatures, however, ocean temperatures underneath the summer mixed layer did not increase significantly. The absolute maximum in summer mixed layer temperatures occurred between 9 and 6 ka BP, representing the Holocene Thermal Maximum in the eastern Nordic Seas. In contrast, maximum in northward oceanic heat transport through the Norwegian Atlantic Current occurred approximately 10 ka BP. The maximum in oceanic heat transport at 10 ka BP occurred due to a major reorganization of the Atlantic Ocean circulation, entailing strong and deep rejuvenation of the Atlantic Meridional Overturning Circulation, combined with changes in the North Atlantic gyre dynamic causing enhanced transport of heat and salt into the Nordic Seas.

Citation: Risebrobakken, B., T. Dokken, L. H. Smedsrud, C. Andersson, E. Jansen, M. Moros, and E. V. Ivanova (2011), Early Holocene temperature variability in the Nordic Seas: The role of oceanic heat advection versus changes in orbital forcing, *Paleoceanography*, 26, PA4206, doi:10.1029/2011PA002117.

1. Introduction

[2] The Holocene Thermal Maximum (HTM) is seen throughout the Northern Hemisphere, in marine and terrestrial reconstructions, and is considered a response to the early Holocene orbital forcing [Renssen *et al.*, 2009]. The timing and magnitude of the HTM are influenced by local and regional feedback mechanisms, e.g., from the atmosphere, ocean, sea ice and vegetation, as well as the impact from disintegrating ice sheets [Crucifix *et al.*, 2002; Helmens *et al.*, 2007; Kaufman *et al.*, 2004]. Traditionally, all reconstructions of warm early to mid-Holocene temperatures at high northern latitudes have been related to the orbital forcing; however, we will show that in the case of the Nordic Seas this view represents an oversimplification.

[3] In the Nordic Seas and surrounding areas, the HTM has been found in a variety of climate archives. Sea surface

temperature (SST) reconstructions based on alkenones and diatoms show warmer than present temperatures in the eastern Nordic Seas approximately 9–6 ka BP [Birks and Koç, 2002; Calvo *et al.*, 2002; Kim *et al.*, 2004; Koç *et al.*, 1993; Rimbu *et al.*, 2004; Risebrobakken *et al.*, 2010]. Thermophilous marine mollusks from raised beach deposits at Spitsbergen show maximum temperatures ~10–9 ka BP [Salvigsen *et al.*, 1992]. Seppä *et al.* [2009] determined Holocene temperatures based on pollen records from 36 sites from two northern European transects. One reached from 57°N (southern Fennoscandia) to 70°N (boreal-arctic boundary in northern Fennoscandia), showing the HTM 8–6 ka BP. Contemporary with the warmest Scandinavian temperatures, the Norwegian glaciers reached their Holocene minimum positions 9–4 ka BP [e.g., Nesje, 2009]. At west Spitsbergen plant macrofossils indicate warmer than present temperatures 9–4 ka BP [Birks, 1991], and local glaciers disappeared 11–5 ka BP [Svendsen and Mangerud, 1997]. At Greenland, borehole temperatures and $\delta^{18}\text{O}$ show a decreasing trend during the Holocene, with the warmest conditions 8–5 and 10–7 ka BP, respectively [Dahl-Jensen *et al.*, 1998; Vinther *et al.*, 2009].

[4] The occurrence of warm early Holocene surface water in the Nordic Seas has been associated with increased northward advection of Atlantic water [Kaufman *et al.*, 2004; Koç *et al.*, 1993]. This view has recently been challenged.

¹Uni Bjerknnes Centre, Uni Research, Bergen, Norway.

²Bjerknnes Centre for Climate Research, University of Bergen, Bergen, Norway.

³Department of Earth Sciences, University of Bergen, Bergen, Norway.

⁴Institute for Baltic Sea Research, Warnemünde, Rostock, Germany.

⁵Shirshov Institute of Oceanology, Moscow, Russia.

Warmer than present temperatures are seen in diatom and alkenone-based SST reconstructions at the Vøring Plateau [Birks and Koç, 2002; Calvo et al., 2002]; however, at the same site there is no evidence for an HTM in temperature reconstructions based on foraminifera and radiolarians [Cortese et al., 2005; Dolven et al., 2002; Risebrobakken et al., 2003]. Jansen et al. [2008] argue that the lack of an HTM in the temperature reconstructions based on foraminifera and radiolarians rules out increased advection as an explanation for the HTM, and that the HTM is solely the response to the radiative forcing due to the orbital configuration at the time. This view has been supported by a comparison of foraminifera-based temperature reconstructions from the Nordic Seas and the North Atlantic [Andersson et al., 2010]. Andersson et al. [2010] show that foraminiferal-based temperature reconstructions, not just from the Vøring Plateau but also from the North Atlantic, record increasing temperatures through the Holocene, contrasting the decreasing summer radiation. They also show that their results are consistent with modeled subsurface mid-Holocene temperatures in the same region [Andersson et al., 2010].

[5] In contrast to the evidence from the North Atlantic and the Vøring Plateau, an early and short-lasting HTM has been reported in temperature reconstructions based on planktic foraminifera from NE Nordic Seas [e.g., Hald et al., 2004, 2007; Sarnthein et al., 2003]. This foraminiferal-based HTM is seen earlier than the HTM recorded by alkenones [Kim et al., 2004; Marchal et al., 2002; Risebrobakken et al., 2010]. Maximum advection of warm Atlantic water and polar amplification of the orbital forcing have been suggested to explain the strong early Holocene temperature signal in the NE Nordic Seas [Hald et al., 2004, 2007; Sarnthein et al., 2003]. These explanations, however, do not account for the discrepancy in timing between different proxies in the same region or the latitudinal discrepancy in timing.

[6] Hence, the cause of the discrepancy in timing of the early Holocene temperature development in the Nordic Seas, between different proxies and with latitude for the same proxies, is still unclear and details unresolved. Therefore it is important to resolve why the proxies disagree, in order to improve our understanding of how different forcing and dynamics, and the interaction between these, influenced the Nordic Seas and surrounding areas during the early Holocene.

[7] We hypothesize that the strong early Holocene summer insolation at high northern latitudes only influenced the summer mixed layer (SML) temperatures in the Nordic Seas, and that these changes cannot be seen as representative for the mean state of the Norwegian Atlantic Current (NwAC), reflecting the oceanic heat advection through the eastern Nordic Seas. Following this hypothesis, the separate roles of orbital forcing and oceanic heat advection must be understood, and the cause of variations in heat advection to the Nordic Seas during the early Holocene must be investigated. Accordingly, we will argue that by separating the response to changes in orbital forcing from the response to variable oceanic heat advection, the discrepancies between early Holocene temperatures in different proxies and at different locations in the Nordic Seas can be explained. Here we want to test this hypothesis by 1) using the 1DICE column model to test the effect of the early Holocene orbital configuration on the Barents Sea temperature, 2) reconstructing SML temperatures by compiling existing alkenone data and 3)

reconstructing the mean state of the NwAC using proxies based on foraminifera. By testing this hypothesis, the link between the southeastern and northeastern Nordic Seas, and the seemingly inconsistent temperature reconstructions, is clarified. Understanding the relative importance of the different forcing and dynamics during HTM also have implications for the discussion on how increased radiative forcing is predicted to cause a future polar amplification and how polar amplification will affect high northern latitudes.

[8] We define HTM as directly related to the early Holocene orbital configuration, entailing stronger-than-present radiative forcing at high northern latitudes that again caused a temperature increase. Hence, in this study the term HTM will further be used only when insolation can be considered the responsible driver behind the recorded temperatures. The main focus of this paper will be on the time period 12–6 ka BP; however, full Holocene records are presented to provide a background reference.

2. Oceanographic Setting and Core Locations

[9] Warm and saline Atlantic water enters the Nordic Seas between Iceland and the Faroe Islands and through the Faroe-Shetland Channel [Orvik and Niiler, 2002]. This warm Atlantic water flows northward in two branches, where the eastern branch of the NwAC follows the shelf edge along Norway (Figure 1). The NwAC bifurcates when it reaches the Barents Sea opening, continuing in the West Spitsbergen Current (WSC) and the North Cape Current (NCaC). The WSC continues northward through the Fram Strait where it submerges underneath Arctic water and continues into the Arctic Ocean. Parts of this subsurface Atlantic water enter the Barents Sea from the Arctic through the Franz-Victoria Trough. The NCaC enters the Barents Sea through the Barents Sea opening (Figure 1). Polar water enters the Nordic Seas from the Arctic Ocean and moves southwards in the East Greenland Current (EGC). There is a strong topographical steering of the main currents in the Nordic Seas [Orvik and Niiler, 2002]. Arctic water, representing a mix of the Polar and Atlantic water, occupies central parts of the Nordic Seas. Atlantic water is separated from Arctic water found further west in the Nordic Seas and northeastward in the Barents Sea by the Arctic front (in the Barents Sea also known as the Polar front [Pfirman et al., 1994]). In the Nordic Seas, the Polar front separates the Polar and Arctic waters.

[10] Atlantic water (7.0–9.5°C; 35.1–35.3 psu) reaches down to a water depth of 400–700 m along the Norwegian and Barents Sea margins. Arctic intermediate water (from 400 to 600 to approximately 1100 m water depth) is seen as a salinity minimum zone (34.7–34.9 psu; –0.5–0.5°C) between the Atlantic water and the deep bottom water (34.91 psu; <0.5°C) [Blindheim and Østerhus, 2005]. The winter mixed layer (WML) reaches down to the interface between Atlantic and intermediate water and is characterized by temperatures around 6°C while the SML reach down to 20–40 m water depth and is characterized by temperatures around 12°C at OWSM (Figure 1) [Nilsen and Falck, 2006]. The interannual variability of the mixed layer temperatures as given from the instrumental time series at OWSM is greater during the summer months, ±1.5°C compared to

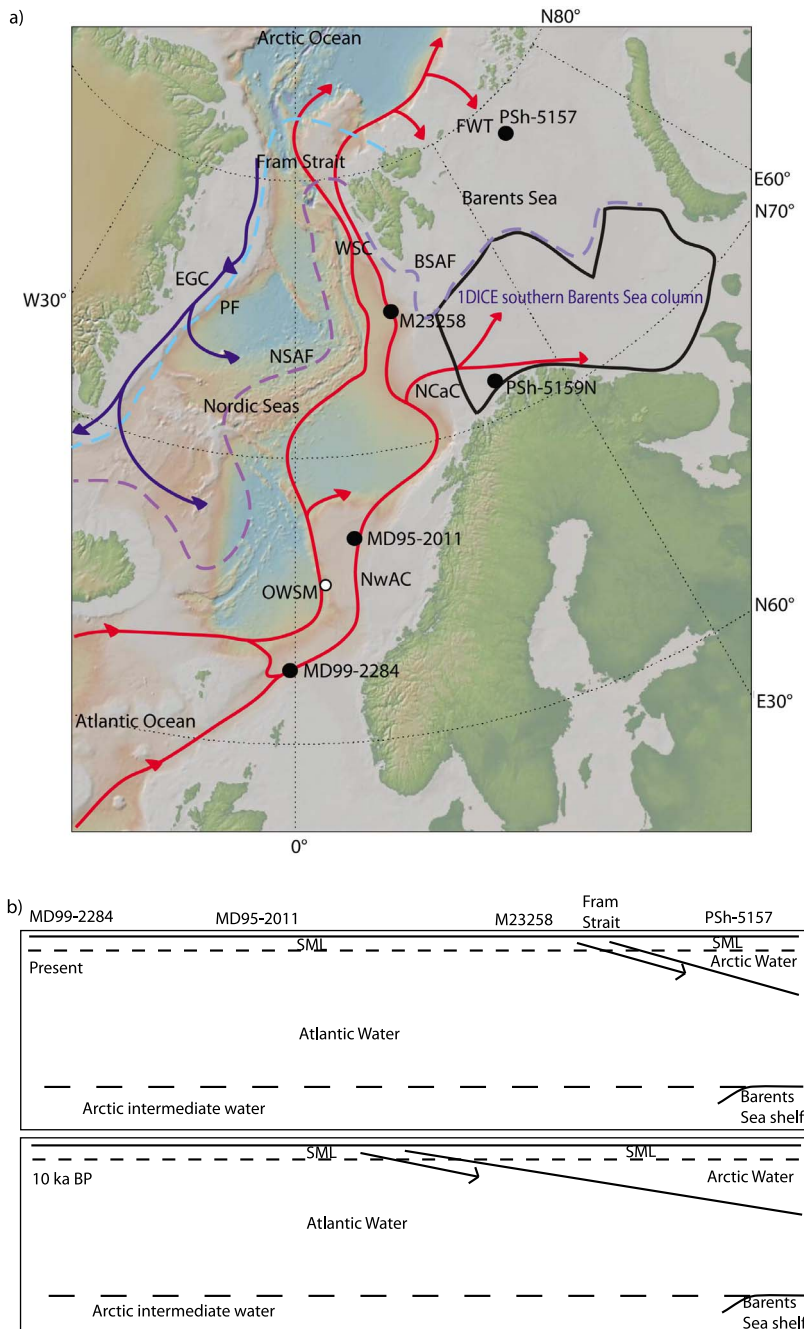


Figure 1. (a) Map showing the location of the discussed core sites. The present-day pathway of Atlantic water through the eastern Nordic Seas and the pathway of Polar water in the western Nordic Seas are indicated. The black line indicates a schematic outline of the southern Barents Sea column used in the 1DICE model experiments. NwAC = Norwegian Atlantic Current. NCaC = North Cape Current. WSC = West Spitsbergen Current. FWT = Franz Victoria Trough. EGC = East Greenland Current. OWSM = Ocean Weather Station Mike. The light purple, stippled line indicates the location of the Nordic Seas Arctic front (NSAF) and the Barents Sea Arctic front (BSAF) (also called Polar front), representing the transition zone between Atlantic and Arctic water masses. The light blue, stippled line indicates the Polar front (PF) that represent the transition zone between Polar and Arctic waters in the western Nordic Seas. (b) A schematic picture of the cross-section showing the water mass structure from the Faroe-Shetland Channel (MD99-2284), past the Vøring Plateau (MD95-2011), the Barents Sea margin (M23258) through the Fram Strait toward the Franz-Victoria Trough (PSh-5157) at present and at 10 ka BP. The arrows indicate submergence of Atlantic water underneath Arctic water.

$\pm 1^{\circ}\text{C}$ in winter. Furthermore, the depth of the SML is more stable than the depth of the WML [Nilsen and Falck, 2006]. Variations in the depth of the WML can be caused by the dynamics of the NwAC related to variable residence time, and degree of convection and entrainment. The NwAC also provide a constant source of heat to the WML, therefore the WML temperature is strongly influenced by the variability of the advective heat flux of the NwAC [Nilsen and Falck, 2006]. Most of the incoming radiation is absorbed in the upper approximately 20–40 m of the water column and the warmer temperature of the SML primarily results from atmospheric heating due to stronger insolation during summer than winter [Nilsen and Falck, 2006]. The thermocline gradually diminishes as mixing occurs during autumn and winter, and the annual mean temperature profiles will normally be comparable to the winter/spring situation. The heat loss from the Atlantic water to the atmosphere increases northward; instrumental records show a decrease in WML temperature by 3–4 $^{\circ}\text{C}$ from 63 $^{\circ}\text{N}$ to 76 $^{\circ}\text{N}$ [Skagseth et al., 2008].

[11] In this paper we will present data from five sites from the eastern Nordic Seas and the Barents Sea: 1) MD99-2284 (Faroe-Shetland Channel, 62 $^{\circ}22.48\text{N}$, 0 $^{\circ}58.81\text{W}$, 1500 m water depth), 2) MD95-2011 (Vøring Plateau, 66 $^{\circ}58.19\text{N}$, 7 $^{\circ}38.36\text{E}$, 1048 m water depth), 3) PSh-5159N (SW Barents Sea, 71 $^{\circ}21.80\text{N}$, 22 $^{\circ}38.77\text{E}$, 422 m water depth), 4) M23258 (Barents Sea margin, 75 $^{\circ}\text{N}$, 14 $^{\circ}\text{E}$, 1768 m water depth) and 5) PSh-5157 (Franz-Victoria Trough, N Barents Sea, 78 $^{\circ}55.48\text{N}$, 41 $^{\circ}52.97\text{E}$, 461 m water depth) (Figure 1). All sites are located underneath the pathway of Atlantic water flowing through the NwAC, the WSC and the NCaC from the southernmost to the northernmost parts of the eastern Nordic Seas, including the inflow to the Barents Sea through the Barents Sea opening and through the Franz Victoria Trough. In the Faroe-Shetland Channel, at the Vøring Plateau and at the Barents Sea margin Atlantic water occupies the upper 400–700 m of the water column, overlaying the Norwegian Sea Arctic intermediate water [Blindheim and Østerhus, 2005]. Deep bottom water characterizes the water column below 1100 m. In SW Barents Sea, Atlantic water occupies the full water column, except for the upper 20–30 m where a mixture of costal and Atlantic water is found [Risebrobakken et al., 2010]. In the Northern Barents Sea, Arctic water occupies the upper 150–200 m of the water column, overlaying Atlantic derived water, and cold bottom water below 300 m. During summer a warm, fresh surface water layer forms in the upper approximately 20 m [Pfirman et al., 1994].

3. Methods

[12] The 1DICE column model was developed and described by Björk [1989]. Here, the southern Barents Sea model setup from Smedsrud et al. [2010] is used. The S Barents Sea area was defined as the sea between northern Norway (71 $^{\circ}\text{N}$) and Bear Island (75 $^{\circ}\text{N}$), and eastward from the Barents Sea margin (20 $^{\circ}\text{E}$) to Novaya Zemlya (Figure 1). The present-day setup of the model has been used; however, the insolation forcing was changed, using horizontally averaged monthly mean insolation at 71 $^{\circ}\text{N}$ for the time slices 12, 11, 10, 9, 8, 7, 6 and 0 ka BP [Laskar et al., 2004]. A planetary albedo of 40% was used to account for the effect of

clouds [Hartmann, 1994]. In 1DICE, a stable annual cycle is usually established within 3 years. For each time slice, the model was therefore run over 10 years with daily time steps to verify that a stable yearly cycle was established. Each run was initiated in August using horizontally averaged profiles of the summer temperature and salinity of the southern Barents Sea, based on available stations in work by Nilsen et al. [2008]. The 1DICE model reproduces the major features of the observed southern Barents Sea annual cycle [Smedsrud et al., 2010].

[13] New planktic foraminiferal census counts were done at the size fraction $>150\ \mu\text{m}$ in 276 samples from MD99-2284 (Faroe-Shetland Channel) and in 130 samples from MD95-2011 (Vøring Plateau), and relative abundances were calculated. The new counts from MD95-2011 were done to optimize the early Holocene resolution (every cm 12–7 ka BP), compared to the previously published early Holocene assemblage data from MD95-2011 (every 5 cm) [Risebrobakken et al., 2003]. The relative abundance of *G. bulloides* in PSh-5159N (SW Barents Sea) is presented for the first time. The samples from PSh-5157 (Franz Victoria Trough) did not contain enough foraminifera to calculate relative abundance. In addition to these new faunal data, previously published relative abundance data from MD95-2011 (supplemented by the new counts) [Andersson et al., 2003; Risebrobakken et al., 2003], M23258 (Barents Sea margin) [Sarnthein et al., 2003] and PSh-5159N (SW Barents Sea) [Chistyakova et al., 2010; Risebrobakken et al., 2010] is presented. In PSh-5159N the census counts are done on the size fraction $>100\ \mu\text{m}$, not at $>150\ \mu\text{m}$.

[14] The Maximum Likelihood (ML) transfer function method [ter Braak and Prentice, 1988; ter Braak and van Dam, 1989] was used to calculate foraminiferal temperatures. This was done for all cores to ensure that all presented foraminiferal temperature records have been calculated in exactly the same manner. The Maximum Likelihood method assumes a unimodal species-environment response model [Telford and Birks, 2005]. The composition of the main species and how each species may influence the temperature estimate is considered when interpreting the results. Furthermore, the counts done at 100 μm (PSh-5159N) may cause temperatures to warm in the cold end, as *T. quinqueloba* is overrepresented at 100 μm compared to 150 μm and the training set used is for 150 μm [Hald et al., 2007; Pflaumann et al., 2003].

[15] New $\delta^{18}\text{O}$ and $\delta^{13}\text{C}$ measurements performed on *Neogloboquadrina pachyderma* (sin) (241 samples) and *Cibicides wuellerstorfi* $\delta^{13}\text{C}$ (134 samples) from MD99-2284 are presented, as well as *N. pachyderma* (sin) $\delta^{18}\text{O}$ from PSh-5157 (216 measurements). All measurements were done in Bergen, using a Finnigan MAT 253 mass spectrometer equipped with an automatic preparation line (“Kiel device”). All foraminifera were crushed and cleaned in methanol, using an ultrasonic bath, before being measured. The foraminifera used for the stable isotope measurements were picked from the 150–500 μm and 106–500 μm fractions in MD99-2284 and PSh-5157, respectively, and the measurements was done on 4–8 *N. pachyderma* (sin) and >2 *C. wuellerstorfi*. The smallest *N. pachyderma* (sin) were avoided when picking from the PSh-5157 samples, as the smaller specimens might cause slightly higher $\delta^{18}\text{O}$ [Hillaire-Marcel et al., 2004]. The PSh-5157 record is considered reliable even

though a minor size effect cannot be excluded. The *N. pachyderma* (sin) $\delta^{13}\text{C}$ record from MD95-2011 corresponds to the MD95-2011 *N. pachyderma* (sin) $\delta^{18}\text{O}$ record published by Risebrobakken *et al.* [2003]. In addition, we present previously published *N. pachyderma* (sin) $\delta^{18}\text{O}$ from MD95-2011 [Risebrobakken *et al.*, 2003], and *N. pachyderma* (sin) $\delta^{18}\text{O}$ and $\delta^{13}\text{C}$ records from PSh-5159N [Risebrobakken *et al.*, 2010] and from M23258 [Sarnthein *et al.*, 2003]. All new and previously published $\delta^{18}\text{O}$ records were corrected for the ice volume effect according to Fairbanks [1989]. The presented $\delta^{18}\text{O}$ records hence reflect a combined temperature and salinity signal.

[16] Further, we have compiled previously published U_{37}^K and $U_{37}^{K'}$ SST records from the sites MD95-2011 [Calvo *et al.*, 2002], M23258 [Marchal *et al.*, 2002; Martrat *et al.*, 2003; J.-H. Kim and R. R. Schneider, GHOST global database for alkenone-derived Holocene sea-surface temperature records, 2004, <http://www.pangaea.de/Projects/GHOST/Holocene>] and PSh-5159N [Risebrobakken *et al.*, 2010]. The alkenone SST records are used as they were originally published. Accordingly, the calibration equation used to calculate SST follow Prahl and Wakeham [1987] for MD95-2011 (U_{37}^K), Rosell-Melé *et al.* [1995] for M23258 ($U_{37}^{K'}$) and Müller *et al.* [1998] for PSh-5159N ($U_{37}^{K'}$). Further details on the methodology and choice of calibration equation behind each U_{37}^K and $U_{37}^{K'}$ SST records can be found in the original publications [Calvo *et al.*, 2002; Martrat *et al.*, 2003; Risebrobakken *et al.*, 2010]. In PSh-5157, there were not enough alkenones to get any signal. No alkenone work has been done on samples from MD99-2284.

[17] The age models of MD99-2284 and PSh-5157 are presented here for the first time. Additional radiocarbon dates are added to the original age model of MD95-2011 [Risebrobakken *et al.*, 2003]. The age models of M23258 and PSh-5159N are based on radiocarbon dates presented by Sarnthein *et al.* [2003] and Risebrobakken *et al.* [2010], respectively. New age models were calculated for all cores to ensure a common chronological framework. The radiocarbon dates was calibrated using Calib 6.0.0 [Stuiver and Reimer, 1993] and the Marine04 calibration data set [Hughen *et al.*, 2004]. For the northern cores (M23258, PSh-5159N and PSh-5157) $\Delta R = 71 \pm 21$ was used [Mangerud *et al.*, 2006], while $\Delta R = 0 \pm 0$ was used for MD99-2284 and MD95-2011. $\Delta R = 200 \pm 50$ was used for all radiocarbon ages within the 11–10 ^{14}C ka interval [Hald *et al.*, 2007]. Vedde Ash and Saksumnavatn Ash ages from Rasmussen *et al.* [2006] were used when these horizons were identified in the sediment. The age models are based on linear interpolation between the tie points given by the calibrated radiocarbon dates and the ash layers (Table 1). Ten dates have been omitted as they gave inverted ages, probably due to influence of resedimented material. Primarily, the dates that provide inverted ages are from the younger parts of the cores, hence, all chronologies are considered reliable for the focus interval of this study.

4. Results

[18] The 1DICE column model is used to investigate the effect of changing insolation forcing at 71°N , at the time slices 12, 11, 10, 9, 8, 7, 6 and 0 ka BP, on temperature profiles representing average conditions in the S Barents

Sea. 1DICE modeled SSTs are consistently higher during the early Holocene than at present (Figure 2a). At 10 ka BP, when the summer insolation forcing reached its Holocene maximum, the modeled August SSTs were 0.6°C higher than at present. The corresponding temperature increase below 20 m water depth is considered insignificant (Figure 2a). Autumn and winter mixing entails a homogeneous S Barents Sea water column. The higher temperatures of the modeled 10 ka SML causes diffusion of some extra heat downward to the deeper water column, but at a very modest level. The amplitude of the 10 ka warming below 60 m depth is a maximum of 0.05°C in July. The rest of the year the difference is smaller than 0.05°C . During the year, the minimum surface mixed layer depth in 1DICE is seen for June through August (~ 12 m), while it rises to a maximum of 58 m in October. The difference in temperature below the mixed layer, between the present and 10 ka, also varies through the year. It is lowest at the end of winter mixing (March, 0.03°C , Figure 2b), and largest at the peak of the insolation (June, 0.05°C , Figure 2b).

[19] The compiled Nordic Seas alkenone SST records provide a consistent picture of the main Holocene trends. The records from the Vøring Plateau (MD95-2011) [Calvo *et al.*, 2002], the SW Barents Sea (Psh-5159N) [Risebrobakken *et al.*, 2010] and the Barents Sea margin (M3258) [Marchal *et al.*, 2002] all shows warm alkenone SSTs during the early to mid-Holocene followed by gradual cooling and maximum temperatures within the 9–6 ka BP interval (Figure 3a). Minor variability, in part of local character, is found superimposed on the main trends. Consistently colder conditions and a larger Holocene temperature decrease are seen at the Barents Sea margin compared to the Vøring Plateau and the SW Barents Sea (Figure 3a). The reconstructed temperature differences between these sites (Vøring Plateau – SW Barents Sea and Vøring Plateau – Barents Sea margin) at 9–6 ka BP are 0.6°C and 5.5°C respectively. These early Holocene temperature differences are within the range of present-day August SST differences between these sites (International Council for the Exploration of the Sea, public oceanographic database, 2010, www.ices.dk).

[20] The main planktic foraminiferal species found in the studied cores during the early Holocene are *N. pachyderma* (sin), *Neogloboquadrina pachyderma* (dex), *Globigerina bulloides* and *Turborotalita quinqueloba* (Figure 4). Renaming *N. pachyderma* (dex) to *Neogloboquadrina incompta* has been suggested [Darling *et al.*, 2006]; however, we use the old name to maintain consistency with previous publications of part of the data discussed. The calculated foraminiferal temperatures reflect the relative abundance of *N. pachyderma* (sin) at all sites (Figure 4); decreases in the relative abundance of *N. pachyderma* (sin) result in warmer estimated temperatures.

[21] Foraminiferal temperatures of the Faroe-Shetland Channel, the Vøring Plateau and the Barents Sea margin record stepwise warming from 12 to 10 ka BP, followed by a cooling toward 9 ka BP (Figures 3c and 4). The temperature peak at 10 ka BP represents the warmest early Holocene foraminiferal conditions. Contemporaneously with the temperature peak at 10 ka BP the relative abundance of *G. bulloides* reached the Holocene maximum level and *N. pachyderma* (dex) occurred in high numbers in the Faroe-Shetland Channel, at the Vøring Plateau and at the

Table 1. Radiocarbon Dates, Ash Horizons and Calibrated Ages Used to Create the Age Models^a

| Lab ID | Core | Sample Depth (cm) | Dated Material | ¹⁴ C Date | ΔR | Calibrated Age Range $\pm 1\sigma$ | Rel. Prob. ^b | Calendar Age BP 1950 (Med. Prob. ^c) | Comment | References for Individual Dates |
|-----------|-----------|-------------------|--|-----------------------------|--------------|------------------------------------|-------------------------|---|----------|--|
| Poz-20001 | PSh-5157 | 7.5 | Bulk foraminifera | 1460 \pm 160 | 71 \pm 21 | 767–1101 | 1 | 942 | Not used | This study |
| | PSh-5157 | 11.5 | Bulk foraminifera | 1170 \pm 30 | 71 \pm 21 | 629–687 | 1 | 659 | Not used | This study |
| Poz-15134 | PSh-5157 | 15.5 | Mollusc | 7490 \pm 40/7540 \pm 50 | 71 \pm 21 | 7837–7932/7868–7982 | 1 | 7883/7930 | Not used | This study |
| Poz-20002 | PSh-5157 | 31 | Bulk foraminifera | 3305 \pm 30 | 71 \pm 21 | 2988–3123 | 1 | 3055 | Not used | This study |
| Poz-36197 | PSh-5157 | 36.5 | Bulk foraminifera | 3135 \pm 35 | 71 \pm 21 | 2767–2874 | 1 | 2830 | | This study |
| Poz-20003 | PSh-5157 | 61 | Bulk foraminifera | 3425 \pm 35 | 71 \pm 21 | 3163–3292 | 1 | 3223 | | This study |
| Poz-20004 | PSh-5157 | 79 | Bulk foraminifera | 4180 \pm 35 | 71 \pm 21 | 4090–4224 | 1 | 4163 | | This study |
| Poz-36198 | PSh-5157 | 100.5 | Bulk foraminifera | 5240 \pm 50 | 71 \pm 21 | 5472–5580 | 1 | 5528 | | This study |
| Poz-15136 | PSh-5157 | 126 | Snail/mollusc | 6380 \pm 40 | 71 \pm 21 | 6709–6836 | 1 | 6769 | | This study |
| Poz-12699 | PSh-5157 | 143 | Yoldia | 6820 \pm 40 | 71 \pm 21 | 7228–7332 | 1 | 7280 | | This study |
| Poz-15137 | PSh-5157 | 168.5 | Mollusc | 7360 \pm 40 | 71 \pm 21 | 7690–7802 | 1 | 7751 | | This study |
| Poz-15138 | PSh-5157 | 220.5 | Mollusc | 9000 \pm 50 | 71 \pm 21 | 9517–9651 | 1 | 9590 | | This study |
| Poz-15130 | PSh-5159N | 7.5 | Mollusc fragments, benthic foraminifera | 102.46_0.32pMC | 71 \pm 21 | | 1 | | | Ivanova et al. [2008] |
| Poz-20399 | PSh-5159R | 14.17 | Lenticulina sp. | 635 \pm 30 | 71 \pm 21 | 174–258 | 0.788 | 197 | | Ivanova et al. [2008] |
| Poz-19995 | PSh-5159N | 21.5 | Bulk foraminifera | 1670 \pm 30 | 71 \pm 21 | 1118–1223 | 1 | 1164 | | Ivanova et al. [2008] |
| Poz-19997 | PSh-5159N | 40.5 | Bulk foraminifera | 2845 \pm 30 | 71 \pm 21 | 2426–2603 | 1 | 2508 | | Risebrobakken et al. [2010] |
| Poz-20568 | PSh-5159N | 45.5 | Bulk foraminifera | 4960 \pm 40 | 71 \pm 21 | 5132–5287 | 1 | 5204 | | Risebrobakken et al. [2010] |
| Poz-15131 | PSh-5159N | 50.5 | Mollusc fragments | 6105 \pm 35 | 71 \pm 21 | 6393–6500 | 1 | 6451 | | Risebrobakken et al. [2010] |
| Poz-19998 | PSh-5159N | 60.5 | Bulk foraminifera | 7040 \pm 40 | 71 \pm 21 | 7423–7507 | 1 | 7472 | | Risebrobakken et al. [2010] |
| Poz-12701 | PSh-5159N | 69.5 | Brachiopod | 7500 \pm 40 | 71 \pm 21 | 7844–7939 | 1 | 7892 | | Risebrobakken et al. [2010] |
| Poz-19999 | PSh-5159N | 86.5 | Bulk foraminifera | 8550 \pm 50 | 71 \pm 21 | 9010–9171 | 1 | 9103 | | Risebrobakken et al. [2010] |
| Poz-15132 | PSh-5159N | 99.5 | Mollusc fragments, benthic foraminifera, ostracode | 9700 \pm 50 | 71 \pm 21 | 10444–10556 | 1 | 10496 | | Risebrobakken et al. [2010] |
| Poz-19991 | PSh-5159R | 122.5 | Mollusc | 10010 \pm 50 | 71 \pm 21 | 10565–10779 | 1 | 10693 | | Risebrobakken et al. [2010]; Chisnyakova et al. [2010] |
| Poz-15133 | PSh-5159N | 133.5 | Mollusc fragments | 10290 \pm 50 | 71 \pm 21 | 11029–11196 | 1 | 11100 | | Risebrobakken et al. [2010] |
| Poz-12629 | PSh-5159N | 148.5 | Astarte crenata | 10360 \pm 50 | 71 \pm 21 | 11118–11217 | 1 | 11165 | | Risebrobakken et al. [2010] |
| Poz-16594 | PSh-5159R | 241 | Bulk benthic foraminifera | 12150 \pm 70 | 71 \pm 21 | 13405–13606 | 1 | 13515 | | Risebrobakken et al. [2010]; Chisnyakova et al. [2010] |
| Poz-19992 | PSh-5159R | 333 | Bulk benthic foraminifera | 13550 \pm 70 | 71 \pm 21 | 15486–16227 | 0.961 | 15813 | | Risebrobakken et al. [2010]; Chisnyakova et al. [2010] |
| KIA7648 | M23258 | 25 | NPS | 1165 \pm 35 | 71 \pm 21 | 622–689 | 1 | 655 | | Sarnthein et al. [2003] |
| KIA7649 | M23258 | 51 | NPS | 2555 \pm 30 | 71 \pm 21 | 2071–2210 | 1 | 2145 | | Sarnthein et al. [2003] |
| KIA7650 | M23258 | 67 | NPS | 3500 \pm 35 | 71 \pm 21 | 3255–3358 | 1 | 3307 | | Sarnthein et al. [2003] |
| KIA7651 | M23258 | 93 | NPS | 4825 \pm 40 | 71 \pm 21 | 4889–5067 | 1 | 5002 | | Sarnthein et al. [2003] |
| KIA11534 | M23258 | 118 | NPD | 6140 \pm 70 | 71 \pm 21 | 6404–6581 | 1 | 6495 | | Sarnthein et al. [2003] |
| KIA7653 | M23258 | 154 | NPS | 7660 \pm 45 | 71 \pm 21 | 7988–8112 | 1 | 8050 | | Sarnthein et al. [2003] |
| KIA7654 | M23258 | 177 | NPS | 8380 \pm 45 | 71 \pm 21 | 8796–8969 | 1 | 8872 | | Sarnthein et al. [2003] |
| KIA8553 | M23258 | 192 | NPS | 8760 \pm 40 | 71 \pm 21 | 9312–9426 | 1 | 9368 | | Sarnthein et al. [2003] |
| KIA11535 | M23258 | 207 | NPD | 8955 \pm 55 | 71 \pm 21 | 9473–9599 | 1 | 9541 | | Sarnthein et al. [2003] |
| KIA9193 | M23258 | 241 | NPS | 9330 \pm 70 | 71 \pm 21 | 9996–10186 | 1 | 10074 | | Sarnthein et al. [2003] |
| KIA8554 | M23258 | 249 | NPS | 9235 \pm 50 | 71 \pm 21 | 9880–10095 | 1 | 9965 | | Sarnthein et al. [2003] |
| KIA9354 | M23258 | 250 | NPS | 9435 \pm 55 | 71 \pm 21 | 10147–10264 | 1 | 10210 | | Sarnthein et al. [2003] |
| KIA7657 | M23258 | 315 | NPS | 10980 \pm 70 | 200 \pm 50 | 12050–12365 | 1 | 12216 | Not used | Sarnthein et al. [2003] |
| KIA7659 | M23258 | 355 | NPS | 12010 \pm 55 | 71 \pm 21 | 13295–13409 | 1 | 13359 | | Sarnthein et al. [2003] |
| KIA 9354 | M23258 | 394 | NPS | 12390 \pm 60 | 71 \pm 21 | 13672–13837 | 1 | 13751 | | Sarnthein et al. [2003] |

Table 1. (continued)

| Lab ID | Core | Sample Depth (cm) | Dated Material | ¹⁴ C Date | ΔR | Calibrated Age Range ±1σ | Rel. Prob. ^b | Calendar Age BP 1950 (Med. Prob. ^c) | Comment | References for Individual Dates |
|-----------|-----------|-------------------|----------------|----------------------|----------|--------------------------|-------------------------|---|------------------|---------------------------------|
| Poz-8245 | MD95-2011 | 5 | NPD | 1020 ± 100 | 0 ± 0 | 519-665 | 1 | 600 | Not used | This study |
| GifA96471 | MD95-2011 | 10.5 | NPD | 980 ± 60 | 0 ± 0 | 526-619 | 1 | 573 | Not used | Risebrobakken et al. [2003] |
| KIA 5600 | MD95-2011 | 24.5 | NPD | 1590 ± 40 | 0 ± 0 | 1102-1215 | 1 | 1153 | Not used | Risebrobakken et al. [2003] |
| KIA 3925 | MD95-2011 | 30.5 | NPD | 1040 ± 40 | 0 ± 0 | 590-649 | 0.789 | 611 | Not used | Risebrobakken et al. [2003] |
| KIA 5601 | MD95-2011 | 47.5 | NPD | 1160 ± 30 | 0 ± 0 | 667-727 | 1 | 703 | Not used | Risebrobakken et al. [2003] |
| Poz-8244 | MD95-2011 | 55.5 | NPD | 1530 ± 90 | 0 ± 0 | 976-1174 | 1 | 1085 | Not used | This study |
| KIA 3926 | MD95-2011 | 70.5 | NPD | 1460 ± 50 | 0 ± 0 | 941-1057 | 1 | 1008 | Not used | Risebrobakken et al. [2003] |
| KIA 6286 | MD95-2011 | 89.5 | NPD | 1590 ± 30 | 0 ± 0 | 740-838 | 1 | 796 | Not used | Risebrobakken et al. [2003] |
| Poz-8246 | MD95-2011 | 102 | NPD | 1790 ± 60 | 0 ± 0 | 1275-1390 | 1 | 1338 | Not used | This study |
| KIA 3927 | MD95-2011 | 130.5 | NPD | 2350 ± 40 | 0 ± 0 | 1912-2029 | 1 | 1970 | Not used | Risebrobakken et al. [2003] |
| KIA 6287 | MD95-2011 | 154 | NPD | 2335 ± 25 | 0 ± 0 | 1888-2000 | 1 | 1953 | Not used | Risebrobakken et al. [2003] |
| GifA96472 | MD95-2011 | 170.5 | NPD | 2620 ± 60 | 0 ± 0 | 2190-2360 | 1 | 2301 | Not used | Risebrobakken et al. [2003] |
| Poz-8242 | MD95-2011 | 225 | NPD | 3000 ± 50 | 0 ± 0 | 2724-2822 | 1 | 2775 | Not used | This study |
| Poz-8241 | MD95-2011 | 250 | NPD | 3380 ± 70 | 0 ± 0 | 3162-3339 | 1 | 3246 | Not used | This study |
| KIA 10011 | MD95-2011 | 269.5 | NPD | 3820 ± 35 | 0 ± 0 | 3711-3823 | 1 | 3769 | Not used | This study |
| Poz-8240 | MD95-2011 | 300 | NPD | 4080 ± 70 | 0 ± 0 | 4006-4224 | 1 | 4122 | Not used | Risebrobakken et al. [2003] |
| KIA 463 | MD95-2011 | 320.5 | NPD | 4330 ± 50 | 0 ± 0 | 4396-4526 | 1 | 4464 | Not used | Risebrobakken et al. [2003] |
| Poz-8238 | MD95-2011 | 451 | NPD | 6420 ± 160 | 0 ± 0 | 6729-7111 | 1 | 6906 | Not used | This study |
| KIA 464 | MD95-2011 | 520.5 | NPD | 7260 ± 60 | 0 ± 0 | 7657-7788 | 1 | 7725 | Not used | Risebrobakken et al. [2003] |
| Poz-8237 | MD95-2011 | 528.5 | NPD | 7690 ± 110 | 0 ± 0 | 8035-8274 | 1 | 8154 | Not used | This study |
| Poz-8236 | MD95-2011 | 533.5 | NPD | 8530 ± 160 | 0 ± 0 | 8988-9377 | 1 | 9154 | Not used | This study |
| Poz-8235 | MD95-2011 | 541.5 | ? | 8280 ± 140 | 0 ± 0 | 8618-8994 | 1 | 8822 | Not used | This study |
| Poz-8234 | MD95-2011 | 570.5 | ? | 8700 ± 90 | 0 ± 0 | 8618-8994 | 1 | 9362 | Not used | This study |
| TUa-3315 | MD95-2011 | 703.5 | NPS | 10775 ± 85 | 200 ± 50 | 11629-12051 | 0.958 | 11805 | Vedde Ash | Risebrobakken et al. [2003] |
| | | 709.5 | Tephra | | | | | 12170 | | Risebrobakken et al. [2003] |
| TUa-3316 | MD95-2011 | 730.5 | NPS | 11875 ± 140 | 0 ± 0 | 13174-13429 | 1 | 13320 | | Risebrobakken et al. [2003] |
| KIA465 | MD95-2011 | 750.5 | NPS | 12220 ± 90 | 0 ± 0 | 13578-13752 | 0.788 | 13635 | | Risebrobakken et al. [2003] |
| KIA3519 | MD95-2011 | 813.5 | NPS | 13450 ± 90 | 0 ± 0 | 15247-15969 | 0.926 | 15760 | | Risebrobakken et al. [2003] |
| KIA-10676 | MD99-2284 | 2.5 | NPS | 1690 ± 30 | 0 ± 0 | 1222-1283 | 1 | 1251 | | Dreger [1999] |
| Poz-10150 | MD99-2284 | 19.5 | NPS | 3515 ± 35 | 0 ± 0 | 3355-3438 | 1 | 3399 | | This study |
| Poz-10151 | MD99-2284 | 36.5 | NPS | 5295 ± 35 | 0 ± 0 | 5601-5686 | 1 | 5649 | | This study |
| Poz-10157 | MD99-2284 | 53.5 | NPS | 7300 ± 40 | 0 ± 0 | 7707-7814 | 1 | 7762 | | This study |
| Poz-33098 | MD99-2284 | 71.5 | NPS | 7940 ± 70 | 0 ± 0 | 8334-8476 | 1 | 8405 | | This study |
| TUa-3301 | MD99-2284 | 100.5 | NPS | 8680 ± 85 | 0 ± 0 | 9261-9451 | 1 | 9343 | | Bakke et al. [2009] |
| Poz-33098 | MD99-2284 | 165.5 | NPS | 9340 ± 90 | 0 ± 0 | 10074-10319 | 1 | 10181 | | This study |
| | | 185.5 | Tephra | | | | | 10350 | Saksurnavatn Ash | |
| TUa-3302 | MD99-2284 | 213.5 | NPS | 10050 ± 95 | 200 ± 50 | 10584-10915 | 1 | 10779 | | Bakke et al. [2009] |
| TUa-3304 | MD99-2284 | 249.5 | NPS | 10700 ± 90 | 200 ± 50 | 11546-11874 | 0.723 | 11654 | | Bakke et al. [2009] |
| | | 362.5 | Tephra | | | | | 12170 | Vedde Ash | |
| Poz-29526 | MD99-2284 | 423.5 | NPS | 11440 ± 80 | 0 ± 0 | 12799-12986 | 0.733 | 12912 | | This study |

^aNPD = *N. pachyderma* (dex), NPS = *N. pachyderma* (sin).

^bRelative probability.

^cMedian probability.

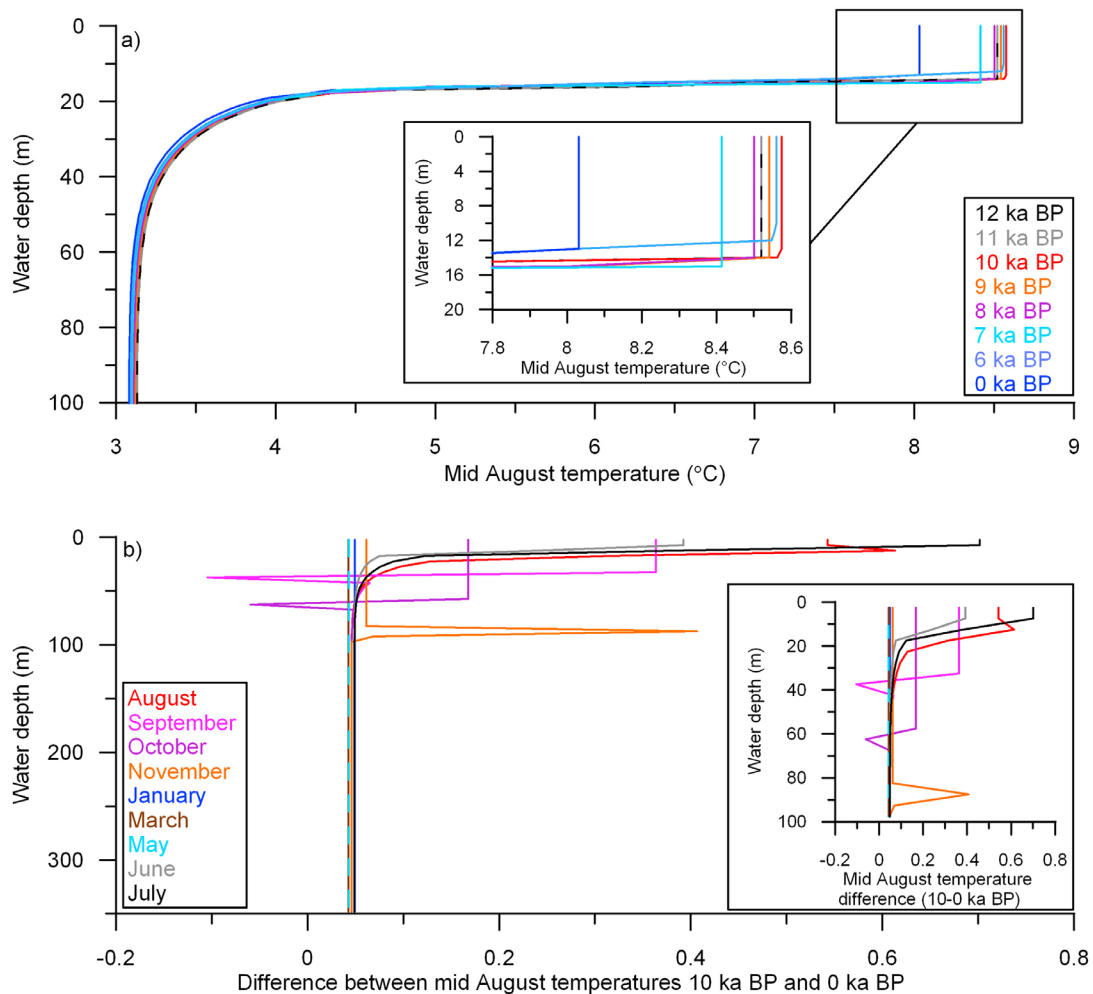


Figure 2. Vertical profiles of temperature for the southern Barents Sea column as calculated by the 1DICE model. (a) Mid August temperature profiles for the years 12, 11, 10, 9, 8, 7, 6 and 0 ka BP. The difference in temperature are solely caused by the difference in monthly mean solar radiation at 71°N for the respective years. The influence of higher increased summer insolation is close to zero for all years below the mixed layer. A blowup of the temperature differences seen in the upper part of the water column is shown in the black box. (b) Difference in temperatures between 10 and 0 ka BP for selected months. The increased insolation at 10 ka BP warms the mixed layer effectively down to a maximum depth of 90 m. The “spikes” at the bottom of the mixed layer are caused by differences in mixed layer depths between the years. A blowup of the upper 100 m is shown in the black box.

Barents Sea margin (Figure 4). At the Barents Sea margin [Sarnthein et al., 2003], more *N. pachyderma* (dex) is found in relation to the early Holocene foraminiferal temperature maximum than anytime later, in contrast to the Faroe-Shetland Channel and the Vøring Plateau where the early Holocene relative abundance of *N. pachyderma* (dex) is significantly lower than during the late Holocene (Figure 4). The relative abundance of *T. quinqueloba* also peaks in the Faroe-Shetland Channel and at the Barents Sea margin during this early Holocene maximum in foraminiferal temperatures. At the Barents Sea margin, *T. quinqueloba* is the most dominant species [Sarnthein et al., 2003]. *Turborotalita quinqueloba* is highly abundant also at the Vøring Plateau; however, at the Vøring Plateau the relative abundance of *T. quinqueloba* remained at the Holocene maximum level throughout the 11–6 ka BP interval (Figure 4). With the

exception of *T. quinqueloba* at the Vøring Plateau, the relative abundance of *G. bulloides*, *N. pachyderma* (dex) and *T. quinqueloba* decreases 10–9 ka BP at the Faroe-Shetland Channel, the Vøring Plateau and the Barents Sea margin (Figure 4).

[22] In the SW Barents Sea, gradually increasing SSTs are indicated 11–7.5 ka BP, followed by cooling, instead of the temperature maximum at 10 ka seen at the Faroe-Shetland Channel, the Vøring Plateau and the Barents Sea margin (Figure 4). The differences in foraminiferal temperature between the SW Barents Sea and the other cores are reflected by the relative abundance data. During the early Holocene, the planktic foraminiferal fauna of the SW Barents Sea was dominated by *T. quinqueloba* (Figure 4) [Chistyakova et al., 2010; Risebrobakken et al., 2010]. *Neogloboquadrina*

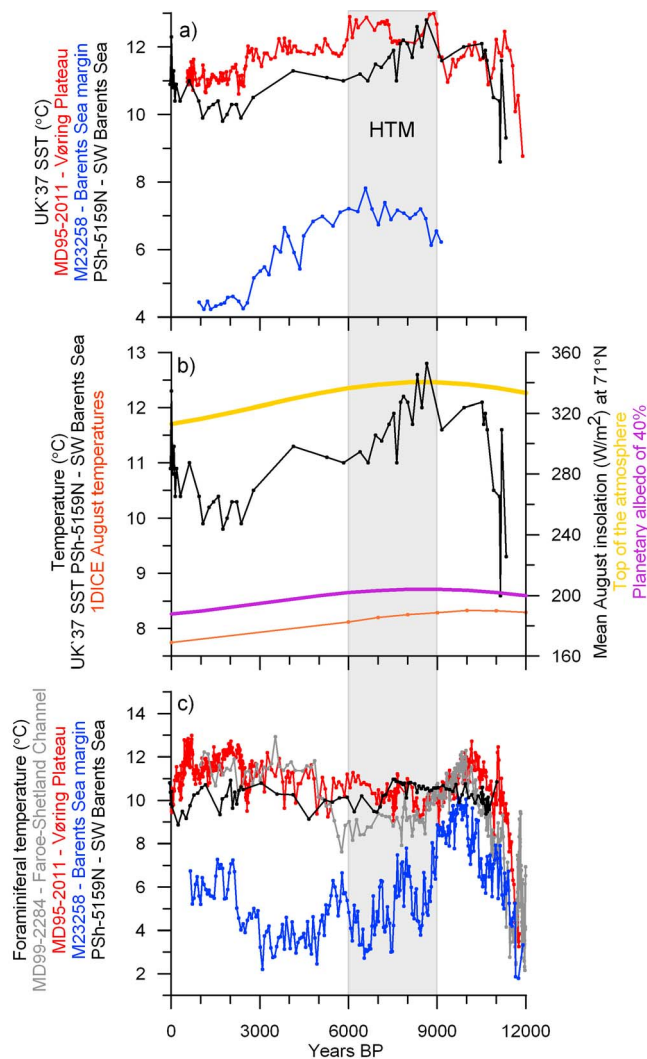


Figure 3. (a) Alkenone SSTs from MD95–2011 (red) [Calvo *et al.*, 2002], PSh–5159N (black) [Risebrobakken *et al.*, 2010] and M23258 (blue) [Marchal *et al.*, 2002]. (b) Alkenone SST of PSh–5159N [Risebrobakken *et al.*, 2010] (black) and 1DICE modeled August temperatures (vertical mean 0–17 m water depth) (red brown) compared to the mean August insolation at the top of the atmosphere (yellow) [Laskar *et al.*, 2004] and the mean August insolation after correcting for a planetary albedo of 40% (purple) [Hartmann, 1994]. (c) Foraminiferal temperatures calculated for this study using the Maximum Likelihood method. MD99–2284 (gray), MD95–2011 (red), PSh–5159N (black) and M23258 (blue). The light gray bar indicates HTM as given by the alkenone SST records.

pachyderma (sin) and *N. pachyderma* (dex) first play a role from 7.5 ka BP, and *G. bulloides* is of minor influence.

[23] A pronounced low in *N. pachyderma* (sin) $\delta^{18}\text{O}$ is seen in the Faroe–Shetland Channel, at the Vøring Plateau [Risebrobakken *et al.*, 2003] and in the SW Barents Sea [Risebrobakken *et al.*, 2010] between 11 and 9 ka BP (Figure 5), followed by comparable more stable conditions. The low $\delta^{18}\text{O}$ signal is least pronounced in the Faroe–Shetland Channel (Figure 5). Low *N. pachyderma* (sin) $\delta^{18}\text{O}$ is also recorded at the Barents Sea margin in the early

Holocene [Sarnthein *et al.*, 2003]; however, the signal is slightly delayed compared to the timing of the depleted signal in the other cores (Figure 5). At the Barents Sea margin, the early Holocene *N. pachyderma* (sin) $\delta^{18}\text{O}$ depletion, are followed by increasing *N. pachyderma* (sin) $\delta^{18}\text{O}$ values (Figure 5) [Sarnthein *et al.*, 2003]. In the Franz–Victoria Trough a gradual *N. pachyderma* (sin) $\delta^{18}\text{O}$ depletion is recorded from 10 ka BP to approximately 8 ka BP, followed by a gradually heavier *N. pachyderma* (sin) $\delta^{18}\text{O}$ 8–4.2 ka BP (Figure 5).

[24] Between 12 and 11 ka BP, strongly depleted *C. wuellerstorfi* $\delta^{13}\text{C}$ are recorded in the Faroe–Shetland Channel, followed by the heaviest Holocene values recorded 11 to 9.8 ka BP, while the *N. pachyderma* (sin) $\delta^{13}\text{C}$ were higher 12–11 and lower 11–9.8 ka BP (Figure 6). A similar *N. pachyderma* (sin) $\delta^{13}\text{C}$ development took place at the Vøring Plateau, and in the SW Barents Sea [Risebrobakken *et al.*, 2010]. Low *N. pachyderma* (sin) $\delta^{13}\text{C}$ is also recorded at the Barents Sea margin 11–9.8 ka BP, however, the decrease from 12 ka BP is less pronounced than in the other cores (Figure 6) [Sarnthein *et al.*, 2003]. Following this early Holocene depletion, a gradual increase in *N. pachyderma* (sin) $\delta^{13}\text{C}$ is seen at all sites until approximately 3 ka BP.

5. Discussion

5.1. Effect of Increased Summer Insolation on Surface and Subsurface Ocean Temperatures

[25] Today, the shallow SML experiences atmospheric-induced heating due to insolation forcing, while below the depth of the SML rather constant temperatures are seen year-round and the year-to-year temperature changes relates to the NwAC and the variability of its advective heat transport [Nilsen and Falck, 2006]. If today's conditions are representative of the past, the proxies representing the SML will provide information on long-term temperature changes caused by variable radiative forcing, while proxies of annual mean temperature conditions will provide information on changes in heat advection related to the mean state of the NwAC. However, summer insolation was stronger at high northern latitudes during the early Holocene than today (Figure 3b) [Laskar *et al.*, 2004].

[26] The 1DICE results show that only SML temperatures were significantly affected by the higher summer insolation (Figure 2a). The influence of insolation on deeper ocean temperatures was within $\pm 0.05^\circ\text{C}$ of the present and is therefore considered to be insignificant throughout the year (Figure 2b). Similarly, Andersson *et al.* [2010] and Liu *et al.* [2003] investigated the effect of insolation on the water column in the Nordic Seas and in the North Atlantic using Community Climate System Model 3.0 (CCSM3) and a low-resolution general circulation model respectively. In agreement with our results, both studies suggest that seasonal summer warming was restricted to the upper ~ 30 m in the Nordic Seas during the early Holocene.

[27] If the results from 1DICE are indicative of early Holocene conditions, we would expect proxy data for the SML to record a insolation driven HTM. Conversely we would expect proxy data for depths below the seasonal thermocline to be unaffected by early Holocene insolation. Within the study area, coccolithophores bloom during summer [Brown and Yoder, 1994; Smyth *et al.*, 2004], and their

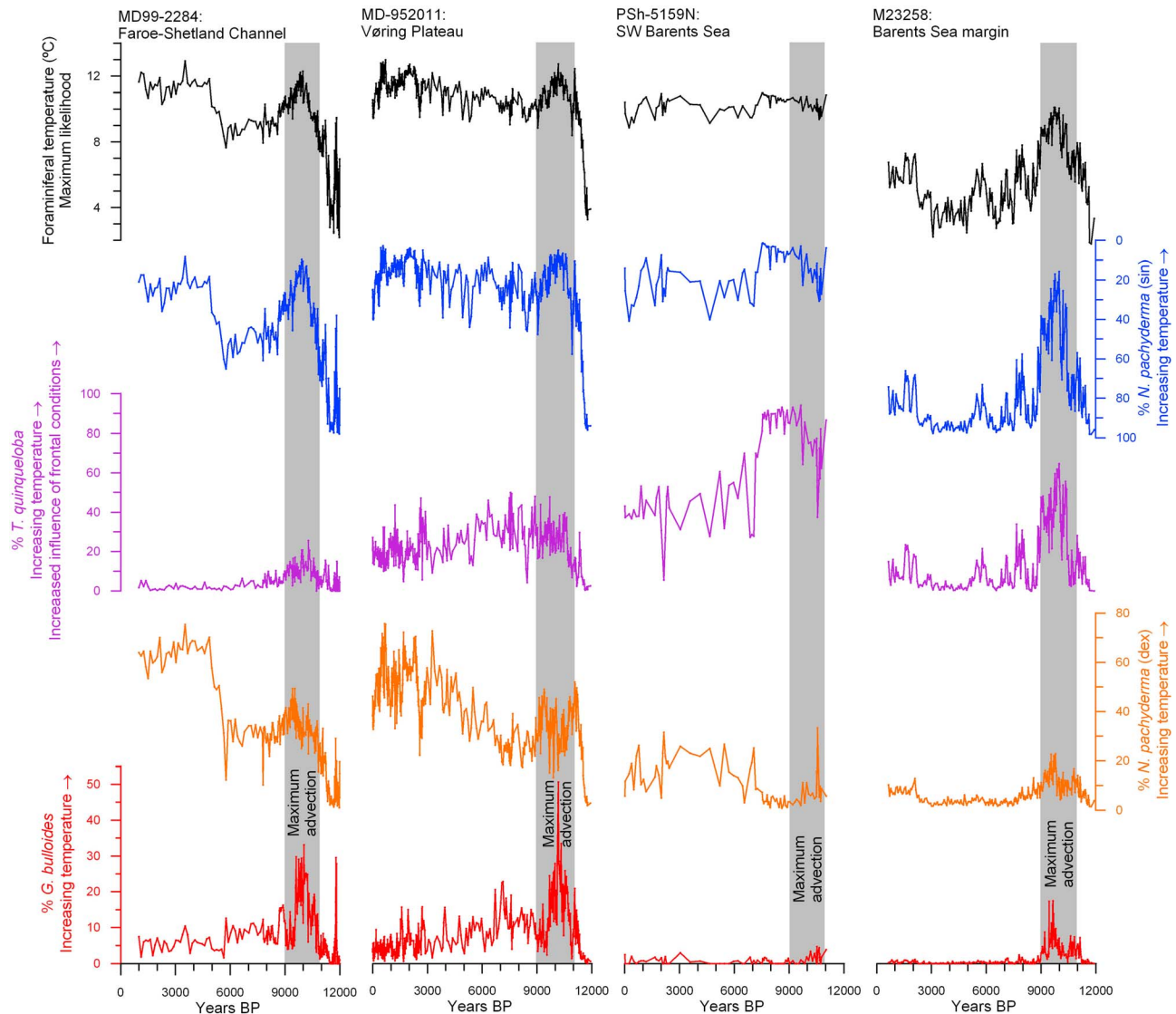


Figure 4. Calculated foraminiferal temperatures, and relative abundance of *N. pachyderma* (sin), *N. pachyderma* (dex), *T. quinqueloba* and *G. bulloides*, from MD99-2284, MD95-2011, PSh-5159N and M23258 are shown. All MD99-2284 data is from this study. The relative abundance data from MD95-2011 represents a combination of new counts done for this study and previously published counts [Andersson *et al.*, 2003; Risebrobakken *et al.*, 2003]. With exception of the relative abundance of *G. bulloides*, the assemblage data from PSh-5159N were published by Risebrobakken *et al.* [2010] and Chistyakova *et al.* [2010]. The relative abundance data from M23258 is from Sarnthein *et al.* [2003]. All foraminiferal temperatures were calculated for this study. The gray bar indicates the interval within when early Holocene maximum advection took place, including the increase toward the absolute maximum at 10 ka BP and the following decrease toward the 9 ka BP minimum.

depth habitat is restricted to the photic zone (10–15 m). The long-term decreasing trends in alkenone SSTs at the Vøring Plateau, the Barents Sea margin and in the SW Barents Sea are therefore interpreted to represent the Holocene temperature development of the SML. Hence, the maximum response to enhanced summer insolation on SML temperatures in the eastern Nordic Seas occurred within the 9–6 ka BP interval (Figure 3a). This interpretation of the alkenone SSTs is in line with argumentation given by Jansen *et al.* [2008] and Andersson *et al.* [2010].

[28] The $C_{37:4}$ alkenone is more abundant in the Nordic Seas than at mid to low latitudes and resuspension and lateral advection of alkenone bearing material may take place [e.g., Bendle and Rosell-Melé, 2004]. However, an examination of the alkenone–SST relationship in the Nordic Seas shows that sediment from the Norwegian Sea provides reliable SSTs for the Holocene [Bendle and Rosell-Melé, 2004]. The consistency between the three independent alkenone SST records reported here further supports the use of alkenones in the Nordic Seas for SML reconstructions during the Holocene. Additionally, the warmer SSTs

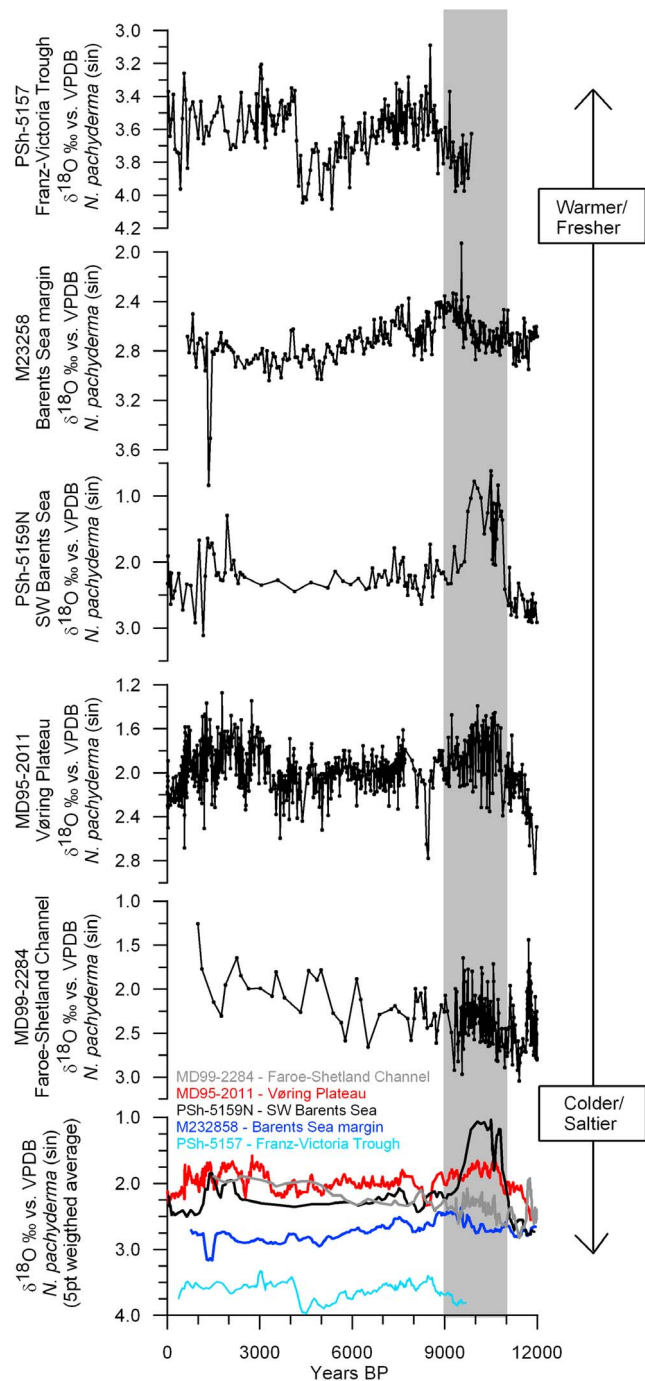


Figure 5. Ice volume corrected $\delta^{18}\text{O}$ of *N. pachyderma* (sin). Smoothed records are shown in the lower panel: MD99-2284 (Faroe-Shetland Channel) (gray), MD95-2011 (Vøring Plateau) (red) [Risebrobakken et al., 2003], PSh-5159N (SW Barents Sea) (black) [Risebrobakken et al., 2010], M23258 (Barents Sea margin) (blue) [Sarnthein et al., 2003] and PSh-5157 (light blue). PSh-5159N [Risebrobakken et al., 2010] and MD95-2011 [Risebrobakken et al., 2003] record more depleted $\delta^{18}\text{O}$ than MD99-2284 during the early Holocene. The gray bar indicates the interval within when early Holocene maximum advection took place, as seen from the foraminiferal temperature and relative abundance data (Figure 4).

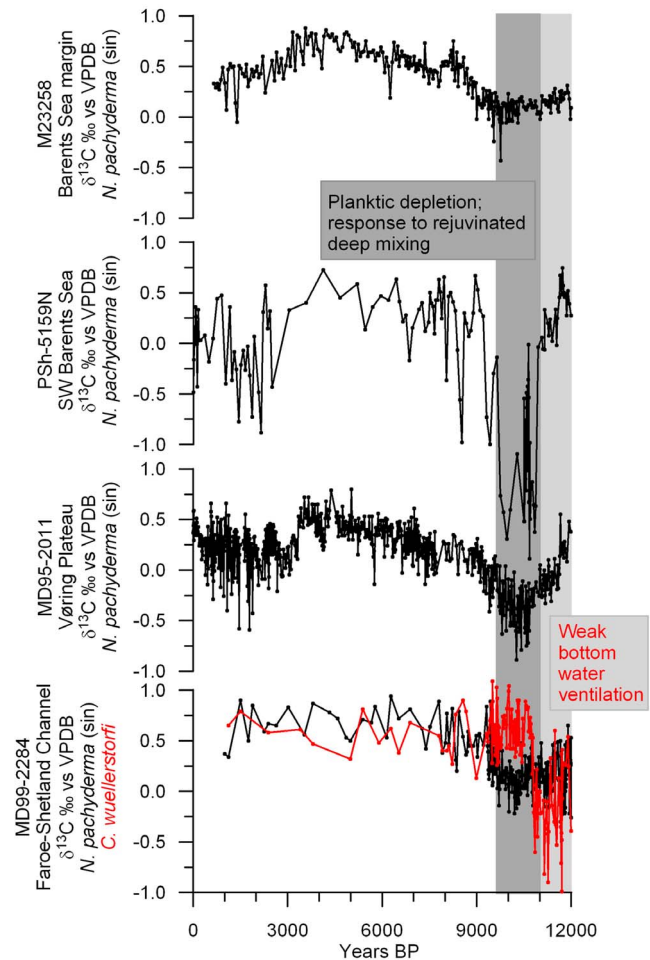


Figure 6. Benthic (*C. wuellerstorfi* - red) $\delta^{13}\text{C}$ from MD99-2284 and planktic (*N. pachyderma* (sin) - black) $\delta^{13}\text{C}$ records from MD99-2284, MD95-2011, PSh-5159N [Risebrobakken et al., 2010] and M23258 [Sarnthein et al., 2003]. The light gray bar represents the interval characterized by extremely light benthic $\delta^{13}\text{C}$ in MD99-2284, indicative of weak ventilation, while the dark gray bar shows the planktic depletion of $\delta^{13}\text{C}$ seen as a response to an initial deep mixing of the water column due to an overshooting AMOC.

reconstructed for the HTM are in agreement with terrestrial records from the same region [e.g., Nesje, 2009; Seppä et al., 2009].

[29] Both 1DICE and SW Barents Sea alkenone SSTs shows an early Holocene temperature maximum followed by a gradual temperature decrease (Figure 3b). The absolute SML temperature maximum is seen 1 ka later in the SW Barents Sea than by 1DICE and the amplitude of change differs. Feedbacks related to disintegrating ice sheets, meltwater, vegetation, sea ice and albedo changes influence the timing and amplitude of the HTM [Kaufman et al., 2004; Otto et al., 2009; Renssen et al., 2009]. 1DICE gives the isolated effect of increased insolation forcing on the ocean temperature in terms of the seasonal and vertical structure for separate time slices compared with the present values, not taking into account any feedback mechanisms. The SW Barents Sea alkenone SSTs shows the temperature devel-

opment with all potential effects from active feedback mechanisms implemented. The time lag and amplitude difference between the modeled and observed Holocene SML temperatures are therefore considered reasonable.

[30] Absolute 1DICE SSTs are lower than the SW Barents Sea alkenone SSTs (Figure 3b). This discrepancy in absolute temperatures reflects that PSh-5159N is located in the warmest part of the Barents Sea, while 1DICE represents mean conditions of the S Barents Sea (Figure 1). The “core top” temperatures of PSh-5159N and 1DICE, 10.9°C and 7.7°C respectively, are comparable with instrumentally recorded August temperatures for the representative location/area, 10.6°C and 8°C respectively [Nilsen *et al.*, 2008; International Council for the Exploration of the Sea, public oceanographic database, 2010].

[31] The Holocene long-term trends and intracore relationships of alkenone SSTs and foraminiferal temperatures differ substantially (Figure 3): 1) None of the sites record higher early Holocene than late Holocene foraminiferal temperatures, with an exception at the Barents Sea margin. 2) An early Holocene maximum in foraminiferal-based temperatures are seen before the maximum in alkenone SSTs. It is therefore reasonable that the two proxies respond to different dynamical forcing. Differences between the proxies have previously been noted at the Barents Sea margin [e.g., Marchal *et al.*, 2002] and at the Vøring Plateau [Andersson *et al.*, 2010; Jansen *et al.*, 2008; Risebrobakken *et al.*, 2003]. Planktic foraminifera are found living over a wide range of water depths; *N. pachyderma* (sin) reflect water at 70–250 m [Simstich *et al.*, 2003], *N. pachyderma* (dex) calcify at approximately 50 m [Nyland *et al.*, 2006], *G. bulloides* dwells in the upper 60 m of the water column [Schiebel *et al.*, 1997] and *T. quinqueloba* calcify at 25–75 m [Simstich *et al.*, 2003]. Furthermore, the season of maximum production differ for different species [Chapman, 2010; Jonkers *et al.*, 2010; Kucera, 2007]. Calculated foraminiferal temperatures integrate information from these different preferential conditions [Andersson *et al.*, 2010]. The deeper living depths of foraminifera compared to coccolithophores causes the foraminifera to record temperatures biased toward annual mean conditions, independent of the calcification season, due the year-round relatively constant temperatures below the SML [Jansen *et al.*, 2008]. A similar relationship is observed in other temperature-sensitive proxies based on foraminifera, e.g., Mg/Ca and $\delta^{18}\text{O}$ reconstructions [Andersson *et al.*, 2010; Leduc *et al.*, 2010]. Since the foraminifera respond to annual mean conditions, these proxies can be used to detect changes in the mean state of the NwAC and accordingly its advection of heat.

[32] To summarize, the early Holocene orbital forcing only influenced SML temperatures in the Nordic Seas. Consequently, only proxies representing SML temperatures record the Nordic Seas HTM documented within the 9–6 ka BP interval. The foraminiferal temperatures record annual mean temperatures and does therefore not see the HTM, however, they do provide a means to detect changes in heat advection through the early Holocene.

5.2. Early Holocene Foraminiferal Assemblages and Temperature Estimates

[33] The high content of *N. pachyderma* (dex) and *G. bulloides* in the Faroe-Shetland Channel, at the Vøring

Plateau and the Barents Sea margin at 10 ka BP demonstrates increased influence of warm Atlantic water (Figure 4). In the Nordic Seas *G. bulloides* and *N. pachyderma* (dex) reflects Atlantic water, with *G. bulloides* as the more warm-loving of the two species [e.g., Bé and Tolderlund, 1971; Johannessen *et al.*, 1994]. For example Hald *et al.* [2007] shows warm foraminiferal temperatures at 10 ka BP close to the Barents Sea, at the Barents Sea margin and at the West Spitsbergen margin, but not at the Vøring Plateau. Here we document this 10 ka BP maximum in foraminiferal temperatures at the Vøring Plateau and in the Faroe-Shetland Channel, hence, the temperature maximum is not restricted to the northeastern Nordic Seas. Following the argumentation from above (4.1), the 10 ka BP warming was a result of intensified heat advection in the NwAC and not related to local heating due to the strong summer insolation anomaly. Hald *et al.* [2007] found that the relative abundance of *G. bulloides* and *N. pachyderma* (dex) was lower at the West Spitsbergen margin than at the Barents Sea margin throughout the 11–9 ka BP interval, indicating a sizable oceanic heat loss before the NwAC entered the Fram Strait.

[34] A minor increase in relative abundance of *G. bulloides* and *N. pachyderma* (dex) in the SW Barents Sea, compared to Barents Sea margin (Figure 4), shows that at 10 ka BP more of the advected heat followed the WSC rather than the NwAC, or that the core of Atlantic water in the NwAC entered the Barents Sea at deeper depths than recorded by planktic foraminifera. Benthic foraminiferal fauna and benthic $\delta^{18}\text{O}$ from the SW Barents Sea document warm bottom water at 10 ka BP, supporting that Atlantic water did enter the Barents Sea [Aagaard-Sørensen *et al.*, 2010; Chistyakova *et al.*, 2010; Risebrobakken *et al.*, 2010].

[35] *Turborotalita quinqueloba* dominates the planktic foraminiferal assemblages in the SW Barents Sea and at the Barents Sea margin 11–7 and 10.5–9 ka BP, respectively [Chistyakova *et al.*, 2010; Risebrobakken *et al.*, 2010; Sarnthein *et al.*, 2003]. *Turborotalita quinqueloba* is a sub-polar species; however, maximum relative abundance occurs near the Arctic front [Johannessen *et al.*, 1994; Matthiessen *et al.*, 2001]. The SW Barents Sea results exemplify how the dual character of *T. quinqueloba* may influence the foraminiferal temperatures when this species dominates the assemblage. The highest foraminiferal temperatures in the SW Barents Sea are recorded 9–8 ka BP, mirroring the relative abundance of *T. quinqueloba*, however, the maximum abundance of *G. bulloides* and *N. pachyderma* (dex) document warmer conditions 11–10 ka BP (Figure 4). Furthermore, warmer foraminiferal temperatures are calculated for the Vøring Plateau and the SW Barents Sea than upstream in the Faroe-Shetland Channel 9–5 ka BP (Figures 3c and 4). Heat is steadily released from the Atlantic water as it moves toward the Arctic [Skagseth *et al.*, 2008]; hence, a northward temperature increase is not realistic. We argue that the too-high downstream temperatures 9–5 ka BP is an artifact of the continuously high content of *T. quinqueloba* at the Vøring Plateau and in the SW Barents Sea compared to the Faroe-Shetland Channel (Figure 4). In agreement, Risebrobakken *et al.* [2003, 2010] found that the Arctic front was located closer to the Vøring Plateau than today and the Barents Sea front was located in vicinity of the SW Barents Sea and the Barents Sea margin through the early to-mid Holocene.

[36] Independent of the front versus temperature discussion, the Holocene maximum in relative abundance of the warm loving *G. bulloides* and *N. pachyderma* (dex) provides clear evidence of NwAC temperatures, and hence northward heat advection, peaking at 10 ka BP (Figure 4). This maximum in heat advection corresponds in time with the early Holocene establishment of a warm mollusk fauna at Spitsbergen [Salvigsen et al., 1992]. Colder foraminiferal conditions are reflected by the reduced relative abundance of *G. bulloides* and *N. pachyderma* (dex) (Figure 4) from 9 to 6 ka BP, when the warmest alkenone SSTs are recorded (Figure 3) [Calvo et al., 2002; Marchal et al., 2002; Risebrobakken et al., 2010], underlining that the different proxies respond to different dynamical mechanisms.

[37] Knudsen et al. [2004] found the highest Holocene content of subpolar planktic foraminifera off North Iceland at ~10 ka BP, reflecting enhanced advection of Atlantic water through the Irminger Current. Maximum in alkenone SST is recorded 10–9 ka off North Iceland, slightly earlier than at the Vøring Plateau [Bendle and Rosell-Melé, 2007], emphasizing the importance of local feedbacks in determining the exact timing of the HTM [Kaufman et al., 2004]; however, the long-term trends are comparable [Bendle and Rosell-Melé, 2007]. Hence, the relationship between early Holocene advection and insolation response off Iceland and in the eastern Nordic Seas is comparable.

5.3. Early Holocene Meltwater Influence

[38] Following a northward oceanic heat release [Skagseth et al., 2008], higher $\delta^{18}\text{O}$ are expected northward if solely influenced by temperature. This is not the case 12–8.5 ka BP; lower $\delta^{18}\text{O}$ are recorded in the SW Barents Sea and at the Vøring Plateau than in the Faroe-Shetland Channel (Figure 5). Accordingly, low-salinity water influenced the Vøring Plateau and SW Barents Sea 12–8.5 ka BP, with a gradually diminishing effect (Figure 5). Supporting the interpretation of reduced salinity, Moros et al. [2004] document ice rafting at the Vøring Plateau 12–8.5 ka BP. Hence, salinity did at times influence the Holocene $\delta^{18}\text{O}$ at the Vøring Plateau, contrasting the argumentation of Risebrobakken et al. [2003]. Maximum heat advection at ~10 ka BP corresponds with low $\delta^{18}\text{O}$ at all sites (Figure 5). In view of that, temperature did play an additional role in defining the $\delta^{18}\text{O}$ signature. In agreement with northward cooling, consistently higher Holocene $\delta^{18}\text{O}$ is recorded at the Barents Sea margin and in the Franz-Victoria Trough than at the upstream sites (Figure 5).

[39] 11–9.5 ka BP the low $\delta^{18}\text{O}$, and hence the influence of low-salinity water, is larger in the SW Barents Sea than at the Vøring Plateau (Figure 5). The SW Barents Sea $\delta^{18}\text{O}$ depletion is explained by melting and refreezing of sea ice after favorable preconditioning [Risebrobakken et al., 2010]. Such a mechanism cannot explain the low salinities at the Vøring Plateau, as the Vøring Plateau site is located further from land and at much deeper water depths than the SW Barents Sea site. The Fennoscandian Ice Sheet (FIS) covered most of Norway, Sweden and Finland at 12 ka BP [Andersen et al., 1995], while remnant ice covered smaller parts of mainland Norway than today's glaciers at 8 ka BP [Nesje, 2009]. Consequently, gradually less fresh water was released to the study area within the time interval 12–8 ka BP. We argue that the early Holocene low-salinity signal at

the Vøring Plateau reflects a direct influence of meltwater, or an expansion of the coastal water, following the final disintegration of the FIS. Reduced early Holocene salinities is also documented in the North Atlantic following deglaciation of the northern Hemisphere ice sheets, with a primary influence from the Laurentide ice sheet [Came et al., 2007; Solignac et al., 2008; Thornalley et al., 2009]. Since both the Nordic Seas and the North Atlantic were influenced by meltwater during the early Holocene, it is reasonable that also the Faroe-Shetland Channel to some extent was affected by fresher surface water.

[40] No salinity response comparable to the Vøring Plateau and SW Barents Sea signal occurred at the Barents Sea margin [Sarnthein et al., 2003] (Figure 5). Today, Atlantic water submerges underneath Arctic water in the Fram Strait [Manley, 1995]. If the submerging zone was located further south the thermocline depth at the Barents Sea margin could have been deeper than today, at a time when today's circulation pattern in the Northern Nordic Seas was not yet established [Risebrobakken et al., 2010]. The thermocline depth represents the upper calcification depth of *N. pachyderma* (sin) [Simstich et al., 2003]. Hence, the lack of fresh water influence on the Barents Sea margin $\delta^{18}\text{O}$ can be explained by a deeper calcification depth of *N. pachyderma* (sin) along the Barents Sea margin than at the Vøring Plateau and in the SW Barents Sea, in combination with a distal location from the main source of fresh water to the Nordic Seas during the early Holocene. The Barents Sea Ice Sheet disintegrated faster than the FIS, and the melting-refreezing mechanism suggested for the shallower and more sheltered Barents Sea [Risebrobakken et al., 2010] would not influence the more open ocean Barents Sea margin.

5.4. Early Holocene Changes in Northward Oceanic Heat Advection Through the NwAC

[41] We have documented that the foraminiferal temperature peak at ~10 ka BP can be followed from the Nordic Seas entrance to the Barents Sea margin (Figure 4), and we argue that it reflects intensified heat advection in the NwAC, independent of local heating due to stronger summer insolation. Furthermore, we will argue that this early Holocene northward propagating warm pulse occurred as a response to a reorganization of the region's climatic state during the last phase of deglaciation and the early Holocene.

[42] During deglaciation of the Northern Hemisphere ice sheets, large amounts of meltwater entered the Nordic Seas and the North Atlantic. Depending on when, where and at what rate meltwater hit the ocean the deglacial fresh water flux can weaken the Atlantic Meridional Overturning Circulation (AMOC) [e.g., Liu et al., 2009; Mignot et al., 2007]. Several studies show that tropical and north Atlantic subsurface water temperature increase in association with an AMOC slowdown [e.g., Barker et al., 2009; Manabe and Stouffer, 1997; Rühlemann et al., 1999]. In the North Atlantic/Nordic Seas, it is suggested that a temperature inversion built up and was maintained due to the influence of deglacial fresh water [Knorr and Lohmann, 2007; Liu et al., 2009]. A surplus reservoir of heat and salt in the tropical and subtropical North Atlantic subsurface were then available for northward advection when the ice sheets diminished, the meltwater flux decreased and the North Atlantic convection sites rejuvenated [Manabe and Stouffer,

1997]. A succeeding rapid salinity recovery in the Polar regions probably broke the temperature inverted density structure causing an destabilization of the Nordic Seas water column [Knorr and Lohmann, 2007; Mignot et al., 2007], resulting in an intensified AMOC, characterized by deeper and stronger circulation than today [Liu et al., 2009; Manabe and Stouffer, 1997]. The subsurface layer cooled rapidly through air-sea interactions, and the convection gradually weakened as the reservoir dampened [Mignot et al., 2007]. We argue that the 10 ka BP maximum in foraminiferal temperatures resulted from such an intensified northward advection of warm water, following an overshoot of the AMOC (Figures 3, 4, and 5). In the Faroe-Shetland Channel, the early Holocene heat pulse is preceded by an interval of extremely light benthic $\delta^{13}\text{C}$ (Figure 6), implying weak ventilation and overturning circulation. Destabilization of the Nordic Seas water column initiated deep mixing that entailed lowering of the planktic $\delta^{13}\text{C}$, as some of the $\delta^{13}\text{C}$ depleted bottom water from the Faroe-Shetland Channel was welled up (Figure 6). Following the NwAC the low *N. pachyderma* (sin) $\delta^{13}\text{C}$ signal propagated northward, influencing all sites (Figure 6). At the same time, the $\delta^{13}\text{C}$ of the bottom water in the Faroe-Shetland Channel increased due to the intensified mixing. Potentially, increased turbulence and upwelling of nutrients related to the intensified mixing also influenced the high early Holocene relative abundance of *T. quinqueloba* (Figure 4).

[43] As the Atlantic reservoir of surplus heat and salt rapidly emptied [Manabe and Stouffer, 1997], the strength of the overturning and the northward heat advection diminished, entailing cooling at all sites after the peak warmth at approximately 10 ka BP (Figure 4). The continuous flux of low salinity water that influenced the Nordic Seas during the early Holocene (Figure 5) was not strong enough to prevent overturning after initial AMOC rejuvenation.

[44] Bakke et al. [2009] hypothesized that the atmospheric jet flickered between a southerly location of the storm tracks, directing the westerlies toward central Europe, and a northern location directing the westerlies toward the Nordic Seas during the late Younger Dryas. Risebrobakken et al. [2003] argued for strong westerlies directed toward the Nordic Seas during the early Holocene. Episodic intrusions of warmer waters into the Nordic Seas coincided with the northward displacement of the storm tracks [Bakke et al., 2009], evidence further supported by a North Atlantic temperature reconstruction [Thornalley et al., 2010]. Fawcett et al. [1997] emphasize the importance of oceanic heat flux into the Nordic Seas in driving the Younger Dryas/Preboreal transition; reducing the sea ice extent moves the winter storm tracks northward. The effect of North Atlantic oceanic heat transport were larger for wintertime than summertime conditions, emphasizing the role the deeper WML and its influence on the regional climate [Alley et al., 1999].

[45] Meltwater freshened the North Atlantic surface water through the deglaciation and early Holocene, affecting interaction between the subpolar gyre (SPG) and the subtropical gyre (STG) [Thornalley et al., 2009]; weakening the SPG due to freshening strengthens the STG and intensifies the transport of heat and salt into the Nordic Seas [Hátún et al., 2005]. Accordingly, the deglacial to early Holocene gyre dynamics enhanced the transport of warmer and salty water into the Nordic Seas.

[46] Summarizing, stronger heat advection into the Nordic Seas at 10 ka BP than before and after took place following a reorganization of the AMOC after the deglaciation, combined with a gyre dynamic causing enhanced transport of heat and salt. A northward displacement of the storm tracks toward the Nordic Seas helped maintaining the enhanced poleward heat transport. As the effect of deglacial preconditioning and meltwater influence on the gyre dynamic diminished, the northward heat transport gradually decreased after ~10 ka BP.

[47] In the Franz-Victoria Trough, *N. pachyderma* (sin) $\delta^{18}\text{O}$ document a temperature maximum at ~8 ka BP (Figure 5), corresponding in time with the HTM recorded by alkenones, not with the foraminiferal temperatures recorded at the other studied sites. In agreement with our record, Duplessy et al. [2001] show a low in Franz-Victoria Trough *N. pachyderma* (sin) $\delta^{18}\text{O}$ 7.85–6.9 ka BP. *Neogloboquadrina pachyderma* (sin) prefer temperate Atlantic water in the NE Fram Strait [Carstens et al., 1997]. Accordingly, *N. pachyderma* (sin) $\delta^{18}\text{O}$ from the Franz-Victoria Trough reflects conditions at approximately 180 m water depth, corresponding to today's Arctic-Atlantic water interface at the site. A fraction of the Atlantic water that submerges underneath Arctic water in the Fram Strait enters the Barents Sea from the Arctic Ocean through the Franz-Victoria Trough. We argue that the *N. pachyderma* (sin) $\delta^{18}\text{O}$ temperature maximum in the Franz-Victoria Trough at 8 ka BP reflects a subsurface propagation through the Fram Strait and into the Arctic Ocean of the contemporaneously high eastern Nordic Seas SML temperatures, in line with arguments by Duplessy et al. [2001] and Lubinski et al. [2001].

6. Summary and Conclusions

[48] Strong early Holocene summer insolation at high northern latitudes increased the SML temperatures in the Barents Sea and the Nordic Seas. However, no significant temperature increase occurred below the SML. Consequently, only proxy records representing the near surface can be used to reconstruct the response to the orbital forcing and hence the HTM. The alkenone SST records document the HTM within the time interval 6–9 ka BP, in good agreement with the timing of the HTM observed in terrestrial records from the same region.

[49] Proxies providing information on conditions underneath the SML represent the mean state of the NwAC and thus changes in northward heat advection through the Nordic Seas. Warmer than, or as warm as, present conditions are recorded by foraminiferal-based proxies at 10 ka BP, all along the pathway of the NwAC from the Faroe-Shetland Channel in the south to the Barents Sea margin in the northern Nordic Seas. The temperature maximum at 10 ka BP shows intensified heat advection through the NwAC. Our findings emphasize that high latitude radiative forcing is not responsible for the overall conditions of the water column and ocean dynamics.

[50] A major reorganization of the ocean circulation following the deglaciation led to the intensified heat advection peaking at 10 ka BP. We hypothesize that strong meltwater discharge to sensitive areas periodically reduced the strength of the AMOC through the deglaciation, entailing weak ventilation of the Nordic Seas until 11 ka BP and a buildup

of an Atlantic subsurface reservoir of heat and salt. Rejuvenating the AMOC entailed a strong and deep overturning circulation that intensified the early Holocene northward heat advection in the NwAC. As the surplus heat reservoir rapidly emptied, the overturning diminished, reducing the northward heat advection through the Nordic Seas. Predominant deglacial to early Holocene gyre dynamics and atmospheric forcing further enhanced the transport of warm and salty water into the Nordic Seas.

[51] Meltwater from the disintegrating ice sheets and glaciers in vicinity of the study area, as well as melting and refreezing of sea ice, freshened the upper part of the water column 12–8.5 ka BP. The salinity of the upper water column gradually increased, as the glaciers reached their minimum Holocene extent and less fresh water reached the study area. The fresh surface water had an additional stabilizing effect on the SML; however, the effect was not large enough to prevent the overturning circulation after its initial recovery.

[52] **Acknowledgments.** Dagfinn Bøe, Rune Søråas and Odd Hansen are thanked for technical assistance. All data from M23258 was obtained through the PANGAEA database. The MD sites were cored through the IMAGES program by R/V Marion Dufresne, while the PSh cores were collected during a joint SIO RAS/BCCR cruise on R/V Professor Shtokman in 2004. The Research Council of Norway has supported this study through the projects p.nr.171159, POCAHONTAS and ARCTREC. This is publication A357 from the Bjerknes Centre for Climate Research. We thank Thomas Cronin and one anonymous reviewer for comments that significantly improved the manuscript.

References

- Aagaard-Sørensen, S., K. Husum, M. Hald, and J. Knies (2010), Paleooceanographic development in the SW Barents Sea during the Late Weichselian–Early Holocene transition, *Quat. Sci. Rev.*, *29*, 3442–3456, doi:10.1016/j.quascirev.2010.08.014.
- Alley, R. B., A. M. Ágústssdóttir, and P. J. Fawcett (1999), Ice-core evidence of late-Holocene reduction in North Atlantic ocean heat transport, in *Mechanisms of Global Climate Change at Millennial Time Scales*, *Geophys. Monogr. Ser.*, vol. 112, edited by P. U. Clark, R. S. Webb, and L. D. Keigwin, pp. 301–312, AGU, Washington, D. C.
- Andersen, B. G., J. Lundquist, and M. Saarnisto (1995), The Younger Dryas margin of the Scandinavian ice sheet—An introduction, *Quat. Int.*, *28*, 145–146, doi:10.1016/1040-6182(95)00043-I.
- Andersson, C., B. Risebrobakken, E. Jansen, and S. O. Dahl (2003), Late Holocene surface ocean conditions of the Norwegian Sea (Vøring Plateau), *Paleoceanography*, *18*(2), 1044, doi:10.1029/2001PA000654.
- Andersson, C., F. Pausata, E. Jansen, B. Risebrobakken, and R. Telford (2010), Holocene trends in the foraminiferal record from the Norwegian Sea and the North Atlantic, *Clim. Past*, *6*, 179–193, doi:10.5194/cp-6-179-2010.
- Bakke, J., Ø. Lie, E. Heegaard, T. Dokken, G. H. Haug, H. H. Birks, P. Dulski, and T. Nilsen (2009), Rapid oceanic and atmospheric changes during the Younger Dryas cold period, *Nat. Geosci.*, *2*, 202–205, doi:10.1038/ngeo439.
- Barker, S., P. Diz, M. J. Vautravers, J. Pike, G. Knorr, I. R. Hall, and W. S. Broecker (2009), Interhemispheric Atlantic seesaw response during the last deglaciation, *Nature*, *457*, 1097–1102, doi:10.1038/nature07770.
- Bé, A. W. H., and D. S. Tolderlund (1971), Distribution and ecology of living planktonic foraminifera in surface waters of the Atlantic and Indian Oceans, in *The Micropaleontology of the Oceans*, edited by B. M. Funnell and W. R. Riedel, pp. 105–149, Cambridge Univ. Press, Cambridge, U. K.
- Bendle, J., and A. Rosell-Melé (2004), Distributions of U_{37}^K and U_{37}^L in the surface waters and sediments of the Nordic Seas: Implications for paleoceanography, *Geochem. Geophys. Geosyst.*, *5*, Q11013, doi:10.1029/2004GC000741.
- Bendle, J. A. P., and A. Rosell-Melé (2007), High-resolution alkenone sea surface temperature variability on the North Icelandic Shelf: Implications for Nordic Seas palaeoclimatic development during the Holocene, *Holocene*, *17*(1), 9–24, doi:10.1177/0959683607073269.
- Birks, C. J. A., and N. Koç (2002), A high-resolution diatom record of late-Quaternary sea-surface temperatures and oceanographic conditions from the eastern Norwegian Sea, *Boreas*, *31*, 323–344, doi:10.1080/030094802320942545.
- Birks, H. H. (1991), Holocene vegetational history and climatic change in west Spitsbergen—Plant macrofossils from Skardtjøna, an Arctic lake, *Holocene*, *1*(3), 209–218, doi:10.1177/095968369100100303.
- Björk, G. (1989), A one-dimensional time-dependant model for the vertical stratification of the upper Arctic Ocean, *J. Phys. Oceanogr.*, *19*, 52–67, doi:10.1175/1520-0485(1989)019<0052:AODTDM>2.0.CO;2.
- Blindheim, J., and S. Østerhus (2005), The Nordic Seas, main oceanographic features, in *The Nordic Seas: An Integrated Perspective: Oceanography, Climatology, Biogeochemistry, and Modeling*, *Geophys. Monogr. Ser.*, vol. 158, edited by H. Drange et al., pp. 11–38, AGU, Washington, D. C.
- Brown, C. W., and J. A. Yoder (1994), Coccolithophorid blooms in the global ocean, *J. Geophys. Res.*, *99*, 7467–7482, doi:10.1029/93JC02156.
- Calvo, E., J. Grimalt, and E. Jansen (2002), High resolution U_{37}^L sea surface temperature reconstruction in the Norwegian Sea during the Holocene, *Quat. Sci. Rev.*, *21*, 1385–1394, doi:10.1016/S0277-3791(01)00096-8.
- Came, R. E., D. W. Oppo, and J. F. McManus (2007), Amplitude and timing of temperature and salinity variability in the subpolar North Atlantic over the past 10 k y, *Geology*, *35*(4), 315–318, doi:10.1130/G23455A.1.
- Carstens, J., D. Hebbeln, and G. Wefer (1997), Distribution of planktic foraminifera at the ice margin in the Arctic (Fram Strait), *Mar. Micropaleontology*, *29*, 257–269, doi:10.1016/S0377-8398(96)00014-X.
- Chapman, M. R. (2010), Seasonal production patterns of planktonic foraminifera in the NE Atlantic Ocean: Implications for paleotemperature and hydrographic reconstructions, *Paleoceanography*, *25*, PA1101, doi:10.1029/2008PA001708.
- Chistyakova, N., E. Ivanova, B. Risebrobakken, E. A. Ovsepyan, and Y. S. Ovsepyan (2010), Reconstruction of postglacial environments in the south-western Barents Sea based on foraminiferal assemblages, *Oceanology*, *Engl. Transl.*, *50*(4), 573–581, doi:10.1134/S0001437010040132.
- Cortese, G., J. K. Dolven, K. R. Björklund, and B. A. Malmgren (2005), Late Pleistocene–Holocene radiolarian paleotemperatures in the Norwegian Sea based on artificial neural networks, *Palaeogeogr. Palaeoclimatol. Palaeoecol.*, *224*(4), 311–332, doi:10.1016/j.palaeo.2005.04.015.
- Crucifix, M., M.-F. Loutre, P. Tulkens, T. Fichetef, and A. Berger (2002), Climate evolution during the Holocene: A study with an Earth system model of intermediate complexity, *Clim. Dyn.*, *19*, 43–60, doi:10.1007/s00382-001-0208-6.
- Dahl-Jensen, D., K. Mosegaard, N. Gundestrup, G. D. Clow, S. J. Johnsen, A. W. Hansen, and N. Baling (1998), Past temperatures directly from the Greenland Ice Sheet, *Science*, *282*, 268–271, doi:10.1126/science.282.5387.268.
- Darling, K. F., M. Kucera, D. Kroon, and C. M. Wade (2006), A resolution for the coiling direction paradox in *Neogloboquadrina pachyderma*, *Paleoceanography*, *21*, PA2011, doi:10.1029/2005PA001189.
- Dolven, J. K., G. Cortese, and K. R. Björklund (2002), A high-resolution radiolarian-derived paleotemperature record for the Late Pleistocene–Holocene in the Norwegian Sea, *Paleoceanography*, *17*(4), 1072, doi:10.1029/2002PA000780.
- Dreger, D. (1999), Decadal-to-centennial-scale sediment records of ice advance on the Barents shelf and meltwater discharge into the northeastern Norwegian Sea over the last 40 kyr, Ph.D. dissertation, 80 pp., Christian-Albrechts-Universität, Kiel, Germany.
- Duplessy, J.-C., E. Ivanova, I. Murdmaa, M. Paterner, and L. Labeyrie (2001), Holocene paleoceanography of the northern Barents Sea and variations of the northward heat transport by the Atlantic Ocean, *Boreas*, *30*, 2–16, doi:10.1080/030094801300062220.
- Fairbanks, R. G. (1989), A 17,000-year glacio-eustatic sea level record: Influence of glacial melting rates on the Younger Dryas event and deep-ocean circulation, *Nature*, *342*, 637–642, doi:10.1038/342637a0.
- Fawcett, P. J., A. M. Ágústssdóttir, and R. Alley (1997), The Younger Dryas termination and North Atlantic Deep Water formation: Insights from climate model simulations and Greenland ice cores, *Paleoceanography*, *12*, 23–38, doi:10.1029/96PA02711.
- Hald, M., H. Ebbesen, M. Forwick, F. Godtlielsen, L. Khomeiko, S. Korsun, L. Ringstad Olsen, and T. O. Vorren (2004), Holocene paleoceanography and glacial history of the West Spitsbergen area, Euro-Arctic margin, *Quat. Sci. Rev.*, *23*, 2075–2088, doi:10.1016/j.quascirev.2004.08.006.
- Hald, M., C. Andersson, H. Ebbesen, E. Jansen, D. Klitgaard-Kristensen, B. Risebrobakken, G. R. Salomonsen, M. Sarnthein, H. P. Sejrup, and R. J. Telford (2007), Variations in temperature and extent of Atlantic Water in the Northern North Atlantic during the Holocene, *Quat. Sci. Rev.*, *26*, 3423–3440, doi:10.1016/j.quascirev.2007.10.005.
- Hartmann, D. L. (1994), *Global Physical Climatology*, 411 pp., Academic, San Diego, Calif.

- Hátún, H., A. B. Sandø, H. Drange, B. Hansen, and H. Valdimarsson (2005), Influence of the Atlantic subtropical gyre on the thermohaline circulation, *Science*, *309*, 1841–1844, doi:10.1126/science.1114777.
- Helmens, K. F., J. A. A. Bos, S. Engels, C. J. Van Meerbeek, S. J. P. Bohncke, H. Renssen, O. Heiri, S. J. Brooks, H. Seppä, and B. Wohlfart (2007), Present-day temperatures in northern Scandinavia during the last glaciation, *Geology*, *35*(11), 987–990, doi:10.1130/G23995A.1.
- Hillaire-Marcel, C., A. de Vernal, L. Polyak, and D. Darby (2004), Size-dependent isotopic composition of planktic foraminifera from Chukchi Sea vs. NW Atlantic sediments—Implications for the Holocene paleoceanography of the western Arctic, *Quat. Sci. Rev.*, *23*, 245–260, doi:10.1016/j.quascirev.2003.08.006.
- Hughen, K. A., et al. (2004), Marine04 marine radiocarbon age calibration, 0–26 cal kyr BP, *Radiocarbon*, *46*, 1059–1086.
- Ivanova, E. V., E. A. Ovspeyan, B. Risebrobakken, and A. A. Vetrov (2008), Downcore distribution of living calcareous foraminifera and stable isotopes in the western Barents Sea, *J. Foraminiferal Res.*, *38*(4), 337–356, doi:10.2113/gsjfr.38.4.337.
- Jansen, E., C. Andersson, M. Moros, K. H. Nisancioglu, B. F. Nyland, and R. J. Telford (2008), The early to mid Holocene thermal optimum in the northern North Atlantic and Nordic Seas: The role of seasonal orbital forcing and Holocene century to millennial scale climate events, in *Natural Climate Variability and Global Warming: A Holocene Perspective*, edited by R. W. Battarbee and H. A. Binney, pp. 123–137, Wiley-Blackwell, Oxford, U. K., doi:10.1002/9781444300932.ch5.
- Johannessen, T., E. Jansen, A. Flatøy, and A. C. Ravelo (1994), The relationship between surface water masses, oceanographic fronts and paleoclimatic proxies in surface sediments of the Greenland, Iceland, Norwegian Seas, in *Carbon Cycling in Glacial Ocean: Constraints on the Ocean's Role in Global Change*, edited by R. Zahn et al., pp. 61–85, Springer, New York.
- Jonkers, L., G.-J. A. Brummer, F. J. C. Peeters, M. Hendriks, H. M. van Aken, and M. F. De Jong (2010), Seasonal stratification, shell flux, and oxygen isotope dynamics of left-coiling *N. pachyderma* and *T. quinqueloba* in the western subtropical North Atlantic, *Paleoceanography*, *25*, PA2204, doi:10.1029/2009PA001849.
- Kaufman, D. S., et al. (2004), Holocene thermal maximum in the western Arctic (0–180°W), *Quat. Sci. Rev.*, *23*, 529–560, doi:10.1016/j.quascirev.2003.09.007.
- Kim, J.-H., N. Rambu, S. J. Lorentz, G. Lohmann, S.-I. Nam, S. Schouten, C. Rühlemann, and R. R. Schneider (2004), North Pacific and North Atlantic sea-surface temperature variability during the Holocene, *Quat. Sci. Rev.*, *23*, 2141–2154, doi:10.1016/j.quascirev.2004.08.010.
- Knorr, G., and G. Lohmann (2007), Rapid transitions in the Atlantic thermohaline circulation triggered by global warming and meltwater during the last deglaciation, *Geochim. Geophys. Geosyst.*, *8*, Q12006, doi:10.1029/2007GC001604.
- Knudsen, K. L., H. Jiang, E. Jansen, J. Eiriksson, J. Heinemeier, and M.-S. Seidenkrantz (2004), Environmental changes off North Iceland during the deglaciation and the Holocene: Foraminifera, diatoms and stable isotopes, *Mar. Micropaleontol.*, *50*, 273–305, doi:10.1016/S0377-8398(03)00075-6.
- Koç, N., E. Jansen, and H. Hafliðason (1993), Paleoclimatic reconstructions of surface ocean conditions in the Greenland, Iceland and Norwegian Seas through the last 14 ka based on diatoms, *Quat. Sci. Rev.*, *12*, 115–140, doi:10.1016/0277-3791(93)90012-B.
- Kucera, M. (2007), Planktonic foraminifera as tracers of past oceanic environments, in *Proxies in late Cenozoic paleoceanography*, edited by C. Hillaire-Marcel and A. de Vernal, pp. 213–262, Elsevier, Amsterdam, doi:10.1016/S1572-5480(07)01011-1.
- Laskar, J., P. Robutel, F. Joutel, M. Gastineau, A. C. M. Correia, and B. Levrard (2004), A long-term numerical solution for the insolation quantities of the Earth, *Astron. Astrophys.*, *428*(1), 261–285, doi:10.1051/0004-6361:20041335.
- Leduc, G., R. Schneider, J. H. Kim, and G. Lohmann (2010), Holocene and Eemian sea surface temperature trends as revealed by alkenone and Mg/Ca paleothermometry, *Quat. Sci. Rev.*, *29*, 989–1004, doi:10.1016/j.quascirev.2010.01.004.
- Liu, Z., E. Brady, and J. Lynch-Stieglitz (2003), Global ocean response to orbital forcing in the Holocene, *Paleoceanography*, *18*(2), 1041, doi:10.1029/2002PA000819.
- Liu, Z., et al. (2009), Transient simulation of last deglaciation with a new mechanism for Bølling-Allerød Warming, *Science*, *325*, 310–314, doi:10.1126/science.1171041.
- Lubinski, D. J., L. Polyak, and S. L. Forman (2001), Freshwater and Atlantic water inflow to the deep northern Barents and Kara Seas since ca 13 ¹⁴C ka: Foraminifera and stable isotopes, *Quat. Sci. Rev.*, *20*, 1851–1879, doi:10.1016/S0277-3791(01)00016-6.
- Manabe, S., and R. J. Stouffer (1997), Coupled ocean-atmosphere model response to freshwater input: Comparison to Younger Dryas event, *Paleoceanography*, *12*, 321–336, doi:10.1029/96PA03932.
- Mangerud, J., S. Bondevik, S. Gulliksen, A. K. Hufthammer, and T. Høisæter (2006), Marine ¹⁴C reservoir ages for 19th century whales and molluscs from the North Atlantic, *Quat. Sci. Rev.*, *25*, 3228–3245, doi:10.1016/j.quascirev.2006.03.010.
- Manley, T. O. (1995), Branching of Atlantic Water within the Greenland-Spitsbergen Passage: An estimate of recirculation, *J. Geophys. Res.*, *100*, 20,627–20,634, doi:10.1029/95JC01251.
- Marchal, O., et al. (2002), Apparent long-term cooling of the sea surface in the northeast Atlantic and Mediterranean during the Holocene, *Quat. Sci. Rev.*, *21*, 455–483, doi:10.1016/S0277-3791(01)00105-6.
- Martrat, B., J. O. Grimalt, J. Villanueva, S. van Kreveld, and M. Sarnthein (2003), Climatic dependence of the organic matter contributions in the north eastern Norwegian Sea over the last 15,000 years, *Org. Geochem.*, *34*, 1057–1070, doi:10.1016/S0146-6380(03)00084-6.
- Matthiessen, J., et al. (2001), Distribution of calcareous, siliceous and organic-walled planktic microfossils in surface sediments of the Nordic Seas and their relation to surface-water masses, in *The Northern North Atlantic: A Changing Environment*, edited by P. Schäfer et al., pp. 105–127, Springer, Berlin, doi:10.1007/978-3-642-56876-3_7.
- Mignot, J., A. Ganopolski, and A. Levermann (2007), Atlantic subsurface temperatures: Response to a shutdown of the overturning circulation and consequences for its recovery, *J. Clim.*, *20*, 4884–4898, doi:10.1175/JCLI4280.1.
- Moros, M., K. Emeis, B. Risebrobakken, I. Snowball, A. Kuijpers, J. McManus, and E. Jansen (2004), Sea surface temperatures and ice rafting in the Holocene North Atlantic: Climate influences on northern Europe and Greenland, *Quat. Sci. Rev.*, *23*, 2113–2126, doi:10.1016/j.quascirev.2004.08.003.
- Müller, P. J., G. Kirst, G. Ruhland, I. Vvon Storch, and A. Rosell-Melé (1998), Calibration of the alkenone paleotemperature index UK'37 based on core tops from the eastern South Atlantic and the global ocean (60°N–60°S), *Geochim. Cosmochim. Acta*, *62*(10), 1757–1772, doi:10.1016/S0016-7037(98)00097-0.
- Nesje, A. (2009), Latest Pleistocene and Holocene alpine glacier fluctuations in Scandinavia, *Quat. Sci. Rev.*, *28*, 2119–2136, doi:10.1016/j.quascirev.2008.12.016.
- Nilsen, J. E. Ø., and E. Falck (2006), Variations of mixed layer properties in the Norwegian Sea for the period 1948–1999, *Prog. Oceanogr.*, *70*, 58–90, doi:10.1016/j.poccean.2006.03.014.
- Nilsen, J. E. Ø., H. Hátún, K. A. Mork, and H. Valdimarsson (2008), The NISE dataset, *Tech. Rep. 08-01*, Faeroese Fisheries Lab., Tórshavn, Denmark.
- Nyland, B. F., E. Jansen, H. Elderfield, and C. Andersson (2006), *Neogloboquadrina pachyderma* (dex. and sin.) Mg/Ca and $\delta^{18}\text{O}$ records from the Norwegian Sea, *Geochim. Geophys. Geosyst.*, *7*, Q10P17, doi:10.1029/2005GC001055.
- Orvik, K. A., and P. Niiler (2002), Major pathways of Atlantic water in the northern North Atlantic and Nordic Seas towards Arctic, *Geophys. Res. Lett.*, *29*(19), 1896, doi:10.1029/2002GL015002.
- Otto, J., T. Raddatz, M. Claussen, V. Brovkin, and V. Gayler (2009), Separation of atmosphere-ocean-vegetation feedbacks and synergies for mid-Holocene climate, *Geophys. Res. Lett.*, *36*, L09701, doi:10.1029/2009GL037482.
- Pfirman, S. L., D. Bauch, and T. Gammelsrød (1994), The northern Barents Sea: Water mass distribution and modification, in *The Polar Oceans and Their Role in Shaping the Global Environment: The Nansen Centennial Volume*, *Geophys. Monogr. Ser.*, vol. 85, edited by O. M. Johannessen, R. D. Muench, and J. E. Overland, pp. 77–94, AGU, Washington, D. C.
- Pflaumann, U., et al. (2003), Glacial North Atlantic: Sea-surface conditions reconstructed by GLAMAP 2000, *Paleoceanography*, *18*(3), 1065, doi:10.1029/2002PA000774.
- Prahl, F. G., and S. G. Wakeham (1987), Calibration of unsaturation patterns in long-chain ketone compositions for paleotemperature assessment, *Nature*, *330*, 367–369, doi:10.1038/330367a0.
- Rasmussen, S. O., et al. (2006), A new Greenland ice core chronology for the last glacial termination, *J. Geophys. Res.*, *111*, D06102, doi:10.1029/2005JD006079.
- Renssen, H., H. Seppä, O. Heiri, D. M. Roche, H. Goosse, and T. Fichefet (2009), The spatial and temporal complexity of the Holocene thermal maximum, *Nat. Geosci.*, *2*, 411–414, doi:10.1038/ngeo513.
- Rimbu, N., G. Lohmann, S. J. Lorentz, J.-H. Kim, and R. R. Schneider (2004), Holocene climate variability as derived from alkenone sea surface temperature and coupled ocean-atmosphere model experiments, *Clim. Dyn.*, *23*, 215–227, doi:10.1007/s00382-004-0435-8.
- Risebrobakken, B., E. Jansen, C. Andersson, E. Mjelde, and K. Hevrøy (2003), A high-resolution study of Holocene paleoclimatic and paleocae-

- nographic changes in the Nordic Seas, *Paleoceanography*, 18(1), 1017, doi:10.1029/2002PA000764.
- Risebrobakken, B., M. Moros, E. Ivanova, N. Chistyakova, and R. Rosenberg (2010), Climate and oceanographic variability in the SW Barents Sea during the Holocene, *Holocene*, 20(4), 609–621, doi:10.1177/0959683609356586.
- Rösel-Melé, A., G. Eglinton, U. Pflaumann, and M. Sarnthein (1995), Atlantic core-top calibration of the U_{37}^K index as a sea-surface palaeotemperature indicator, *Geochim. Cosmochim. Acta*, 59(15), 3099–3107, doi:10.1016/0016-7037(95)00199-A.
- Rühlemann, C., S. Mulitza, P. J. Müller, G. Wefer, and R. Zahn (1999), Warming of the tropical Atlantic Ocean and slowdown of thermohaline circulation during the last deglaciation, *Nature*, 402, 511–514, doi:10.1038/990069.
- Salvigsen, O., S. L. Forman, and G. H. Miller (1992), Thermophilous molluscs on Svalbard during the Holocene and their paleoclimatic implications, *Polar Res.*, 11(1), 1–10, doi:10.1111/j.1751-8369.1992.tb00407.x.
- Sarnthein, M., S. van Kreveld, H. Erlenkauser, P. M. Grootes, M. Kucera, U. Pflaumann, and M. Schulz (2003), Centennial-to-millennial-scale periodicities of Holocene climate and sediment injections off the western Barents shelf, 75°N, *Boreas*, 32, 447–461, doi:10.1080/03009480301813.
- Schiebel, R., J. Bijma, and C. Hemleben (1997), Population dynamics of the foraminifer *Globigerina bulloides* from the eastern North Atlantic, *Deep Sea Res., Part I*, 44(9–10), 1701–1713, doi:10.1016/S0967-0637(97)00036-8.
- Seppä, H., A. E. Bjune, R. J. Telford, H. J. B. Birks, and S. Veski (2009), Last nine-thousand years of temperature variability in Northern Europe, *Clim. Past.*, 5, 523–535, doi:10.5194/cp-5-523-2009.
- Simstich, J., M. Sarnthein, and H. Erlenkauser (2003), Paired $\delta^{18}O$ signals of *Neogloboquadrina pachyderma* (s) and *Turborotalita quinqueloba* show thermal stratification structure in Nordic Seas, *Mar. Micropaleontol.*, 48, 107–125, doi:10.1016/S0377-8398(02)00165-2.
- Skagseth, Ø., T. Furevik, R. Ingvaldsen, H. Loeng, K. A. Mork, K. A. Orvik, and V. Ozhigin (2008), Volume and heat transports to the Arctic Ocean via the Norwegian and Barents Sea, in *Arctic-Subarctic Ocean Fluxes*, edited by R. R. Dickson et al., pp. 45–64, Springer, Dordrecht, Netherlands, doi:10.1007/978-1-4020-6774-7_3.
- Smedsrud, L. H., R. Ingvaldsen, J. E. Ø. Nilsen, and Ø. Skagseth (2010), Heat in the Barents Sea: Transport, storage, and surface fluxes, *Ocean Sci.*, 6, 219–234.
- Smyth, T. J., T. Tyrrell, and B. Tarrant (2004), Time series of coccolithophore activity in the Barents Sea, from twenty years of satellite imagery, *Geophys. Res. Lett.*, 31, L11302, doi:10.1029/2004GL019735.
- Solignac, S., M. Grelaud, A. de Vernal, J. Giraudeau, M. Moros, I. N. McCave, and B. Hoogakker (2008), Reorganization of the upper ocean circulation in the mid-Holocene in the northeastern Atlantic, *Can. J. Earth Sci.*, 45, 1417–1433, doi:10.1139/E08-061.
- Stuiver, M., and P. J. Reimer (1993), Extended ^{14}C database and revised CALIB 3.0 ^{14}C age calibration program, *Radiocarbon*, 35, 215–230.
- Svendsen, J. I., and J. Mangerud (1997), Holocene glacial and climatic variations on Spitsbergen, Svalbard, *Holocene*, 7(1), 45–57, doi:10.1177/095968369700700105.
- Telford, R. J., and H. J. B. Birks (2005), The secret assumption of transfer functions: Problems with spatial autocorrelation in evaluating model performance, *Quat. Sci. Rev.*, 24, 2173–2179, doi:10.1016/j.quascirev.2005.05.001.
- ter Braak, C. J. F., and I. C. Prentice (1988), A theory of gradient analysis, *Adv. Ecol. Res.*, 18, 271–317, doi:10.1016/S0065-2504(08)60183-X.
- ter Braak, C. J. F., and H. van Dam (1989), Inferring pH from diatoms: A comparison of old and new calibration methods, *Hydrobiologia*, 178, 209–223, doi:10.1007/BF00006028.
- Thornalley, D. J. R., H. Elderfield, and N. I. McCave (2009), Holocene oscillations in temperature and salinity of the surface subpolar North Atlantic, *Nature*, 457, 711–714, doi:10.1038/nature07717.
- Thornalley, D. J. R., I. N. McCave, and H. Elderfield (2010), Freshwater input and abrupt deglacial climate change in the North Atlantic, *Paleoceanography*, 25, PA1201, doi:10.1029/2009PA001772.
- Vinther, B. M., et al. (2009), Holocene thinning of the Greenland ice sheet, *Nature*, 461, 385–388, doi:10.1038/nature08355.

C. Andersson, T. Dokken, E. Jansen, B. Risebrobakken, and L. H. Smedsrud, Bjerknes Centre for Climate Research, University of Bergen, Bergen N-5007, Norway. (bjorg.risebrobakken@uni.no)

E. V. Ivanova, Shirshov Institute of Oceanology, 36 Nakhimovskiy Prosp., Moscow 117997, Russia.

M. Moros, Institute for Baltic Sea Research, Seestrasse 15, Warnemünde, Rostock D-18119, Germany.